Synthesis and Performance Evaluation of Hydrocracking Catalysts: A Review

Roba Saab[a], Kyriaki Polychronopoulou[a,b,*], Lianxi Zheng[a], S. Kumar[c], Andreas Schiffer[a,*]

[a] *Department of Mechanical Engineering, Khalifa University of Science and Technology, Abu Dhabi, 127788, UAE*

[b] *Center for Catalysis and Separation, Khalifa University of Science and Technology, Abu Dhabi, 127788, UAE*

[c] *James Watt School of Engineering, University of Glasgow, Glasgow, G12 8LT, United Kingdom*

Abstract

This review provides a comprehensive summary of current hydrocracking applications, and presents recent advances in the synthesis and structure/composition control of various nanomaterials used in hydrocracking catalysts. Although a wide range of feeds are considered in this review, particular focus is placed on hydrocracking of aromatic and paraffinic compounds. The significance, concepts and principles of the hydrocracking process are first discussed focusing on its wide range of industrial applications. Then, recent advances in the synthesis of hydrocracking catalysts are presented, including different types of zeolites and metal promoted catalysts. Finally, we compare the performances of a wide range of hydrocracking catalysts, and discuss how their intrinsic properties (e.g. surface area, porosity, acidity, morphology and structure) can be controlled to achieve optimal catalytic performance in hydrocracking of aromatic compounds, heavy petrochemicals, paraffinic hydrocarbons and vegetable oils.

Keywords: hierarchical zeolite; catalysis; hydrocracking; hydroprocessing; fuel; bi-functional catalyst

[*] Corresponding authors: A. Schiffer: andreas.schiffer@ku.ac.ae, Tel: +971 (0)2 401 8204;
K. Polychronopoulou: kyriaki.polychrono@ku.ac.ae, Tel: +971 (0)2 401 8211

1. Introduction

World-wide, petrochemicals and fuels are prepared from coal, petroleum oil and natural gases [1]. Hydrocracking is a process by which heavy petroleum products are converted into lighter chemicals with lower boiling points in the presence of hydrogen and a suitable catalyst. Compared to thermal cracking, hydrocracking is performed at relatively low temperatures [2], has better catalytic activity, and facilitates the conversion of fuels into high-quality products with high hydrogen to carbon ratio and low content of impurities (e.g. metals) [3]. This eliminates the post-treatment processes usually required in thermal cracking and thus reduces the total processing cost significantly [4].

1.1 Hydrocracking applications in the past and the present

Hydrocracking was first developed in Germany between 1915 and 1945 to convert coal into liquid fuels [5]. After World War II, the interest in hydrocracking coal for fuel production decreased with the presence of crude oil in the Middle East. In 1960, a new hydrocracking technology known as 'Isocracking' was developed and commercialized by Chevron Research Company [5]. This significant advancement in hydrocracking was directly linked to the development of zeolite-based catalysts which showed significant improvements in terms of catalytic activity, gasoline selectivity and ammonia tolerance. Until today, zeolite-based catalysts continue to play a dominant role in commercial hydrocracking, particularly de-aluminated and low-sodium, or high-silica type-Y zeolites. These zeolites are often embedded in an amorphous matrix, acting as a binder, and are typically loaded with metals on the zeolite and the matrix [6].

Although hydrocracking is predominantly used in petroleum refining, the rapid advancement of nanotechnology in the last decade has opened new pathways for catalyst synthesis and paved the way towards new hydrocracking applications such as biofuel production from vegetable oils, biomass and municipal solid wastes.

In petrochemical plants, hydrocracking reactors are needed to covert heavy oils (e.g. heavy vacuum gas oils, tar, etc.) into lighter and more useful fuels. Furthermore, hydrocracking is also an effective process to convert by-products of oil refining processes [7] into lighter, high-value products, such as the conversion of polyaromatic hydrocarbons into benzene, toluene and xylene

(BTX) [8]. Although it is often considered a demanding process, various studies have attempted to produce high yield of BTX from hydrocracking of complex aromatic chains [9]–[11].

Due to the ever-increasing demand for renewable energy sources, biofuels have become more and more popular in recent years and are seen as viable alternatives to fossil fuels [12]. However, 95% of the world's biodiesel is currently made from edible oil, which puts the global food supply chain under pressure [13]. Recent studies [14], [15] have demonstrated that hydrocracking processes can be effectively used to convert non-edible vegetable oil into lighter hydrocarbons, thereby providing a promising alternative pathway for biofuel production.

Hydrocracking processes have also been used in the conversion of municipal solid wastes into fuel. Such wastes contain a significant amount of hydrocarbons, originating from food leftovers and plastics. Due to the environmental concerns associated with landfilling or combustion of such wastes, it has been suggested to convert these wastes into useful products such as crude oil through pyrolysis [16]. However, the obtained crude oil cannot be immediately used because of its low fluidity and complex structure, and would rather need further processing [17]. Hydrocracking is a favoured catalytic process to refine such crude oil into lighter fuels [18]. Unlike crude oil from petroleum, the pyrolysis crude oil from municipal waste includes nitrogen and oxygen rich compounds, for which the hydrocracking requires a special catalyst that involves hydrodesulfurization (HDS), hydrodenitrogenation (HDN), and hydrodeasphaltenization (HDA) processes [19]. Hydrocracking is also employed for plastic waste degradation, as the latter gives rise to serious environmental hazards. Zeolite-based catalysts proved to be effective for plastic waste degradation, specifically due to their porosity tuning feature [20], which enables the selection of the optimal zeolite porosity depending on the given reaction required.

Furthermore, hydrocracking of lignin in biomass, a renewable energy source, has become a promising pathway for the production of green fuels [21]. Depolymerization of lignin, which is aromatic in nature [22], is a key process in effectively utilizing biomass which is usually done through gas and liquid phase pyrolysis [23], but the low aromatic product yield and considerable char formation are major drawbacks of these methods [24]. To overcome these issues, metal supported catalysts and zeolites were used in hydrocracking of lignin, reporting significant reductions in char formation and substantial improvements in the yield of liquid products [25]–[30].

The references cited above show that the types of feeds used in hydrocracking processes can vary substantially, and thus, operating conditions (e.g. temperature, hydrogen partial pressure, hourly feed velocity, etc.) widely differ depending on the feed and the desired products. Regardless of the process conditions and feed used, the performance of a hydrocracking process relies on the presence of a bi-functional catalyst which is the focal point of our discussions in the following section.

1.2 The notion of a bi-functional catalyst

Hydrocracking is typically performed using a bi-functional catalyst where the cracking function is provided by the acidic support and hydrogenation-dehydrogenation function is provided by impregnated metals, as shown in Figure 1. The support offers large surface area for catalysis, and enables uniform dispersion of the active metal particles. In general, supports are desirably porous materials with high thermal stability [1].

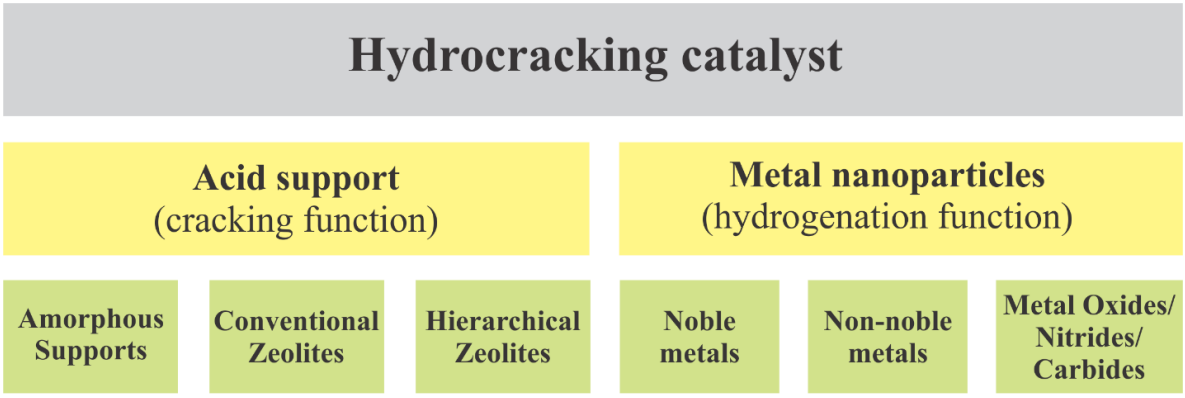

Figure 1. Composition of a bi-functional catalyst for hydrocracking applications

Amorphous silica-alumina as well as conventional and hierarchical zeolites, or combinations thereof, are all potential acidic supports for active noble (e.g. Pt, Pd, etc.) and non-noble (e.g. Co, Ni, Mo, W, etc.) metals. However, zeolites are widely preferred over other supports because of their stronger acidity, higher thermal and hydro-thermal stability, higher resistance to sulfur and nitrogen compounds, reduced coke production tendency and higher regeneration capability [31].

The porosity of zeolites gives rise to their unique shape selectivity characteristic, as certain reactions are facilitated while others are suppressed due to the high or low accessibility of reactants to reaction sites, and slow transport of products out of these sites. Their small pores allow for the diffusion of only small molecules through the pores (see Figure 2), whereas larger molecules can possibly be cracked by the silica-alumina matrix. Variations in catalytic activity and selectivity can potentially reflect differences in cavity sizes and confinement effects, as well as acidity differences. Acidity can significantly influence the selectivity of catalysts. For instance, the distribution of microporous Brönsted acidity affects the shape-selectivity in a catalyst [32], and thus, a balance between acid functions and metal functions can lead to optimal catalytic performance [33]–[36]. Confinement effects can be favourable as with the case of using medium-pore zeolites to easily form aromatics from feeds such as, light paraffins and olefins, with minimal coking rate [31]. Figure 2 schematically illustrates molecule diffusion within macropores, mesopores, and micropores, colored in red, yellow, and green, respectively [37].

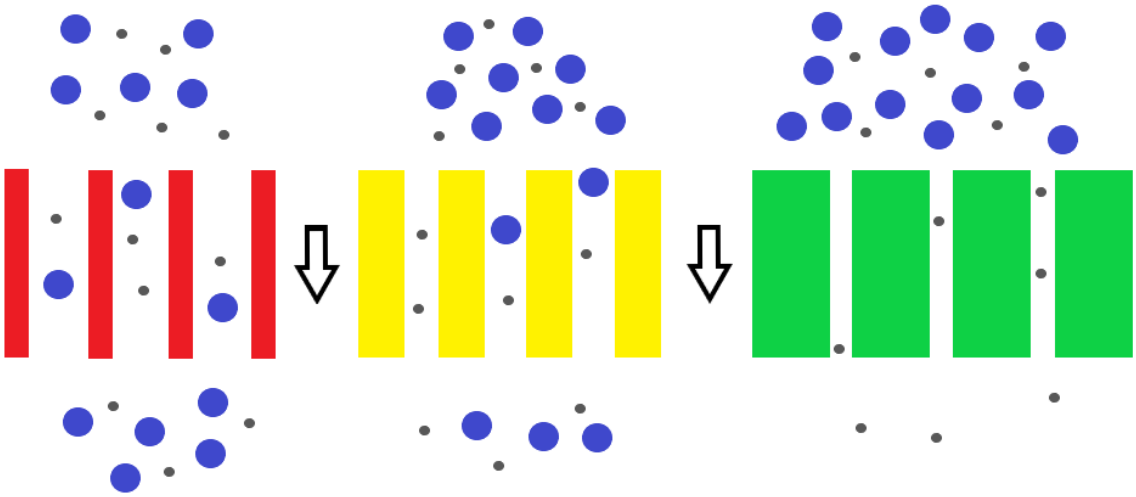

Figure 2. Schematic illustration of the diffusion of molecules within macropores (red), mesopores (yellow), and micropores (green) of a zeolite.

Although the microporosity of zeolite is beneficial in terms of shape selectivity, it has inherent diffusion limitations, resulting in slow mass transport and reduced reaction rates [38]. The

reduction in diffusivity enables the conversion of reagents into undesired by-products (e.g. coke precursors), resulting in blocking of micropores and catalyst deactivation. Subsequently, the external part of the zeolite takes part in the reaction with the internal part being catalytically inactive. To avoid this issue, efforts have been made to synthesize zeolites with hierarchical pore structure involving secondary porosity (often mesopores) to enhance access of larger molecules to active sites, while preserving the zeolite's acidity and crystallinity [38]. Hierarchical pore systems in zeolites can be obtained either through creating intracrystalline mesopores in the microporous zeolite [39], or through a system of carefully tailored nano-sized zeolite crystals [39] that result in intercrystalline mesoporosity (see Section 2.1 for further details). As shown in Figure 3, decreasing the crystal dimensions, and thus the diffusion path length, such as synthesizing nanocrystal zeolites, was reported to improve the catalyst lifetime [37]. Furthermore, introducing additional porosity, at a smaller scale, shortens the diffusion paths and therefore, enhances catalyst lifetime and inhibits catalyst deactivation [37].

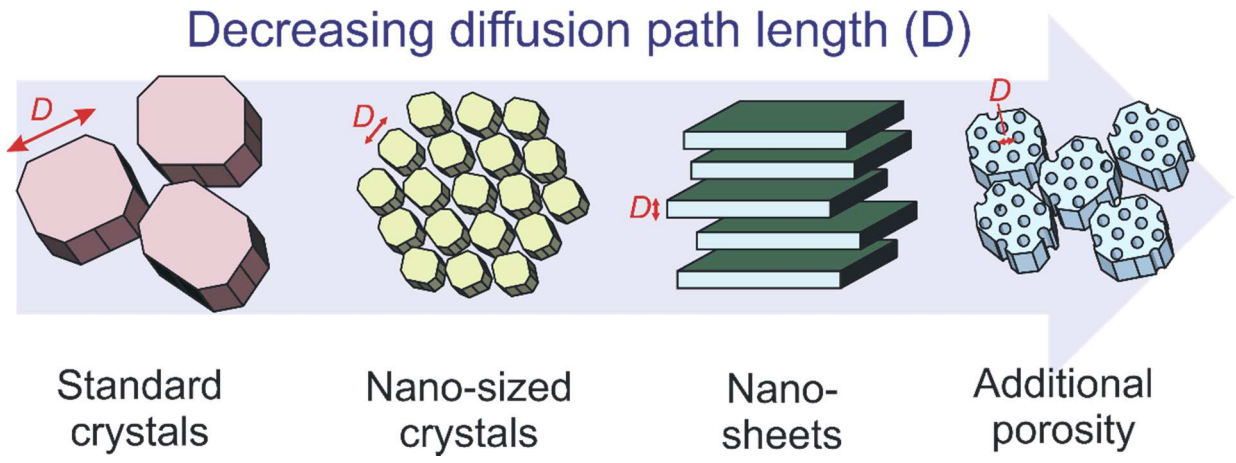

Figure 3. Sketch showing the decrease of diffusion path length in hierarchical zeolites.

1.3 Overview of reaction mechanisms

The details of the hydrocracking chemistry strongly depend on the type of feed used and thus, different reaction mechanisms occur for hydrocracking of paraffinic (alkanes), naphthenic (cycloalkanes) and aromatic (arenes) compounds. To narrow down the focus of the discussion, the

reaction pathways in hydrocracking of paraffinic compounds are explained in detail in the following [40]; for hydrocracking of other types of feeds, the reader is referred to the literature [40].

As sketched in Figure 4, the process starts with physisorption of the feed molecules from the fluid phase into the pore system of the catalyst. The feed molecule then migrates to a metal particle on the zeolite, chemisorbs at its center and then dehydrogenates to an alkene as follows:

$$CH_3CH_2CH_2CH_2CH_2CH_3 \leftrightharpoons CH_3CH=CHCH_2CH_2CH_3 + H_2, \quad (1)$$

The latter alkene leaves the metallic center and migrates to a Brønsted acid site where it is protonated into a carbenium ion according to

$$CH_3CH=CHCH_2CH_2CH_3 \leftrightharpoons CH_3CH_2C^+HCH_2CH_2CH_3, \quad (2)$$

Subsequently, the produced paraffinic carbenium ions undergo isomerization reactions, such as alkyl shifts or protonatedcyclopropane (PCP) steps (see Figure 4), to form more stable isomerized carbenium ions. PCP steps increase the degree of branching in the carbenium ions, e.g.:

$$CH_3CH_2C^+HCH_2CH_2CH_3 \longrightarrow CH_3C^+(CH_3)CH_2CH_2CH_3, \quad (3)$$

Consequently, β-scission of the isomerized carbenium ion takes place to form an olefin and a shorter carbenium ion as follows:

$$CH_3C^+(CH_3)CH_2CH_2CH_3 \longrightarrow CH_3C(CH_3)=CH_2 + C^+H_2CH_3, \quad (4)$$

The olefin can either be further cracked on an acid site of the catalyst, or it can undergo a hydrogenation reaction over a metal particle via

$$CH_3C(CH_3)=CH_2 + H_2 \leftrightharpoons CH_3C(CH_3)HCH_3, \quad (5)$$

The shorter carbenium ions, produced by eq. (4), can be deprotonated on an acid site of the catalyst to form an olefin; e.g.

$$C^+H_2CH_3 \leftrightharpoons CH_2=CH_2 + H^+, \quad (6)$$

The olefins produced by eq. (6) can migrate to a metal particle and form a paraffin through the following hydrogenation reaction

$$CH_2 = CH_2 + H_2 \leftrightharpoons CH_3CH_3, \quad (7)$$

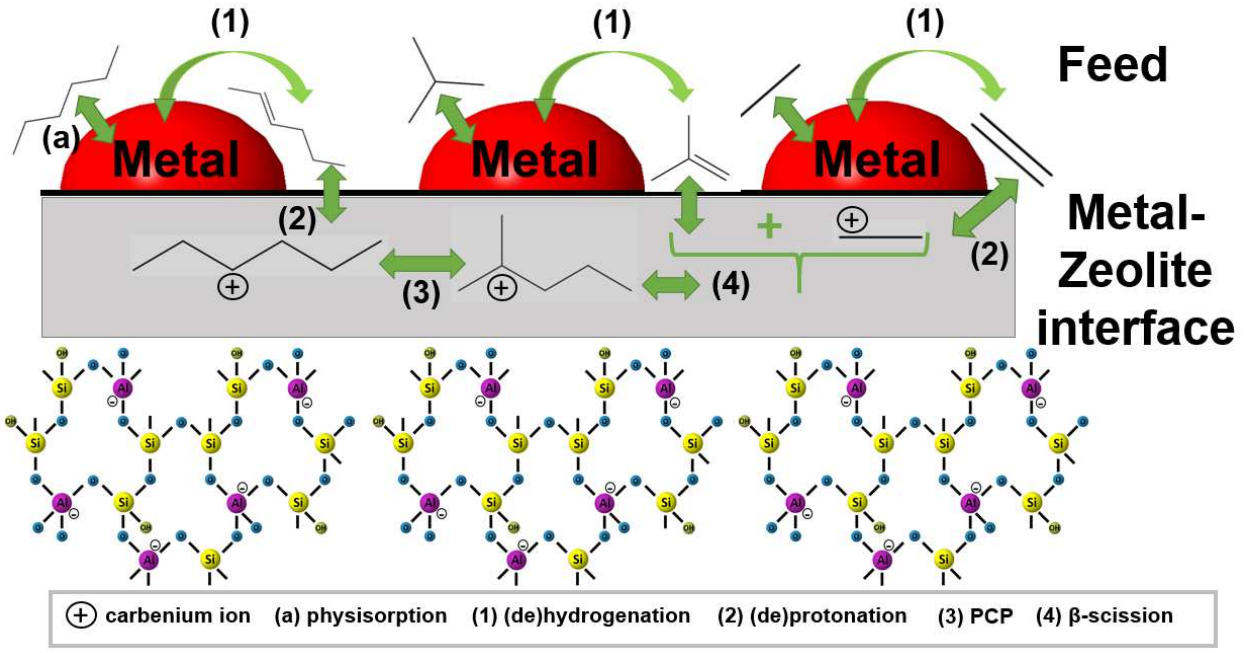

Figure 4. Graphical illustration of the reaction mechanism for hydrocracking of a paraffin (yellow circles: Si, purple circles: Al, blue circles: O, gold circles: OH)

Protonation step, as explained in eq. (2), involves the transformation of an olefin into a carbenium ion by an attack of H^+ at a C=C bond. As compared to other reactions on acid sites, such as PCP and β-scission, this reaction is much faster and is close to equilibrium under commercial operating conditions [41]. The deprotonation step converts carbenium ions to olefins, through the breakage of a C-H bond into H^+ and an olefin. Thus, to analyse these steps from kinetic or thermodynamic perspective, it is important first to understand the nature of the reactive intermediates on acid sites in e.g. zeolite-catalysed hydrocracking in the case of paraffinic carbenium ions. Tertiary alkylcarbenium ions exist in higher concentrations as compared to secondary alkylcarbenium ions due to stability issues. This facilitates the conversion of tertiary alkylcarbenium ions at the highest rates in comparison to the secondary alkylcarbenium ions, even though the activation energies of reactions for the former ions are higher than for the latter ones, which leads to the general

conclusion that reaction pathways through the activation of tertiary carbon atoms proceed at higher rates than reaction pathways through activation on secondary carbon atoms [42]. Kinetic models of hydrocracking of n-octane on Pt/H-USY were carried out based on two contradicting assumptions: the concentration of the reactive intermediates on the acid sites were once considered negligible and once not. The second assumption was closer to experimental data, where the standard protonation enthalpy for tertiary alkylcarbenium ion formation was -94 $kJmol^{-1}$ and that for secondary alkylcarbenium ion formation was -59.2 $kJmol^{-1}$. It was also concluded that the alkylcarbenium ions present in the zeolite channels, reduce the micropore volume available for alkane physisorption. Moreover, variations in physisorption and protonation behavior caused by the different nature of the zeolite used also contribute to the differences in relative alkylcarbenium ion concentrations [42].

Heats of protonation at the surface of the catalyst, ΔH^{sur}, as shown in eq. (8), is the sum of the heats of stabilization of carbenium ions from gas phase to the catalyst surface, ΔH^{gas}, and negative of the relative heat of stabilization of the carbenium ions, Δq, (determined as the difference in the heat of stabilization of a proton and a carbenium ion), and is highly dependent on the acidity of the catalyst [43]:

$$\Delta H^{sur} = \Delta H^{gas} + \Delta q. \tag{8}$$

The entropy of protonation is usually estimated through statistical thermodynamics on the basis of the loss of various degrees of freedom (DOF) in the protonation step. The entropy corresponding to three translational DOFs, S_t, is given by

$$S_t/R = ln(Q_t) + 5/2, \tag{9}$$

where R is the universal gas constant and Q_t is the translational partition function. When protonation occurs, the olefinic and aromatic species from the sorbed phase become attached to the acidic sites, causing the change in the entropy from the sorbed state to the protonated state to become interesting [43]. Further details on mechanistic kinetic modelling of hydrocracking reactions can be found in the literature [44]–[46].

1.4 Scope and structure of this review

In this review paper, we present and discuss the findings of recent studies concerned with the synthesis, characterization and testing of hydrocracking catalysts for upgrading fossil and renewable fuels. Apart from the catalytic results that are presented, this paper also provides a comprehensive overview of the current state-of-the-art in catalyst design and synthesis, and should appeal to the novice and expert alike.

The content of this paper is organized as follows. First, we present recent advances in the synthesis of hydrocracking catalysts with emphasis on the synthesis of meso-porous zeolites. Then, attention is focused on the performance of bi-functional catalysts in hydrocracking of selected types of feeds including aromatic and paraffinic hydrocarbons, heavy petrochemical feedstock and vegetable oil. The discussions highlight the effects of the catalyst's characteristics, such as structure, composition and morphology, on the conversion, yield, selectivity and deactivation resistance of the catalyst. The paper concludes with a summary of the major advances in the design and selection of hydrocracking catalysts including directions for future research in this field.

2. Synthesis of hydrocracking catalysts

Synthesizing a hydrocracking catalyst often involves two major steps, namely synthesis of a support material with acid sites (e.g. zeolite) and subsequent deposition of metal nanoparticles on the support. In the following, we elaborate on both these steps with a focus on the synthesis of zeolites as an acidic support of the catalyst.

2.1 Synthesis of zeolites

In this section, we present an overview of recent advances in the synthesis of zeolites for hydrocracking applications. The discussion includes strategies for creating and tailoring the size, shape and distribution of mesopores in hierarchical zeolites.

Zeolites are crystalline alumino-silicates with a well-defined structure and high surface area. They are essential components of many hydrocracking catalysts since they provide the cracking function through their acid sites (see Section 1.2). A key structural feature of zeolites is their microporosity which results from voids in the crystal lattice formed by the silica-alumina tetrahedral, as shown in Figure 5. Zeolites have been widely used for industrial hydrocracking applications [47] because

of (i) their strong Brønsted acidity due to the bridging OH groups, (ii) their shape selectivity arising from molecular sieving property as a result of the uniform crystal pore sizes, and (iii) being relatively environmentally friendly compared to other acidic catalysts [31]. The most widely used zeolite in industrial hydrocracking is the Y-type zeolite (part of the Faujasite zeolite family) treated post-synthetically to obtain the ultra-stable form with higher Si/Al ratio and enhanced thermal stability [31]. Bifunctional catalysts based on ultra-stable zeolite-Y (USY) were tested for cyclohexane hydrocracking under industrially relevant hydrocracking conditions, in an attempt to quantify the inhibition of Brønsted acid sites caused by nitrogen-containing molecules [48]. The results demonstrated that under the chosen reaction conditions, the fraction of inhibited Brønsted sites exceeded 98% due to the adsorption of ammonia, showing that the Brønsted sites are nearly saturated by NH_3 molecules. Alternatively, raising the temperature from 600 to 640K triplicated the amount of vacant Brønsted sites due to the significant endothermicity of ammonia desorption. The effect of temperature on the inhibition of acid sites by NH_3 is zeolite dependent, particularly, related to the zeolite structure and composition through the number and strength of acid sites [48].

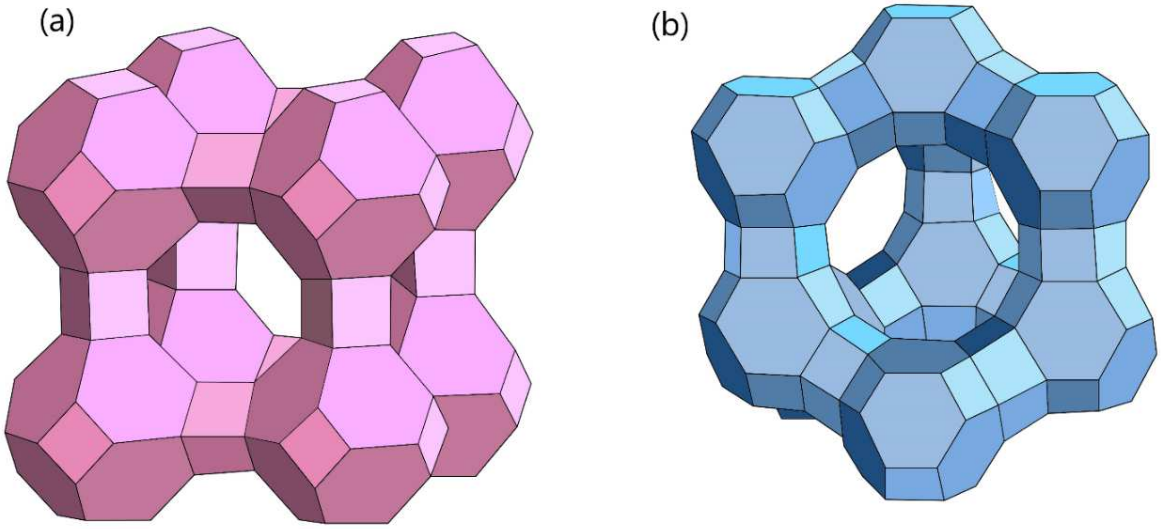

Figure 5. Representative zeolite frameworks: (a) zeolite A, (b) zeolite Y

Synthesis of conventional (microporous) zeolites commonly involves hydrothermal crystallization of alumina-silicate gels, or solutions in basic medium [49]. The majority of zeolites is crystallized in mediums having pH values ranging from 9 to 13, where the OH^- anions act as catalysts for the mineralization process. Increased alkalinity is required to reach the supersaturated state, decreasing the induction period while increasing both nucleation and growth rate, leading to a decrease in the Si/Al ratio [50]. Moreover, silicate species in aluminosilicate gels become more deprotonated at increased alkalinity reducing the condensation rate.

Recent studies have focused on the synthesis of hydrocracking catalysts composed of zeolites with hierarchically porous architecture, enhancing the catalyst's surface area and facilitating access to larger molecules at the active sites of the zeolite. As shown in Figure 6, hierarchical zeolites can be obtained either by creating inter- or intra-crystalline hierarchical pore systems. We refer to inter-crystalline mesoporosity, if the mesopores are represented by the spaces between adjacent zeolite crystals, while in case of intra-crystalline mesoporosity, the periodic arrangement of atoms in the zeolite is interrupted by larger holes that are obtained, for example, by selectively removing atoms from the lattice structure of the microporous zeolite [39].

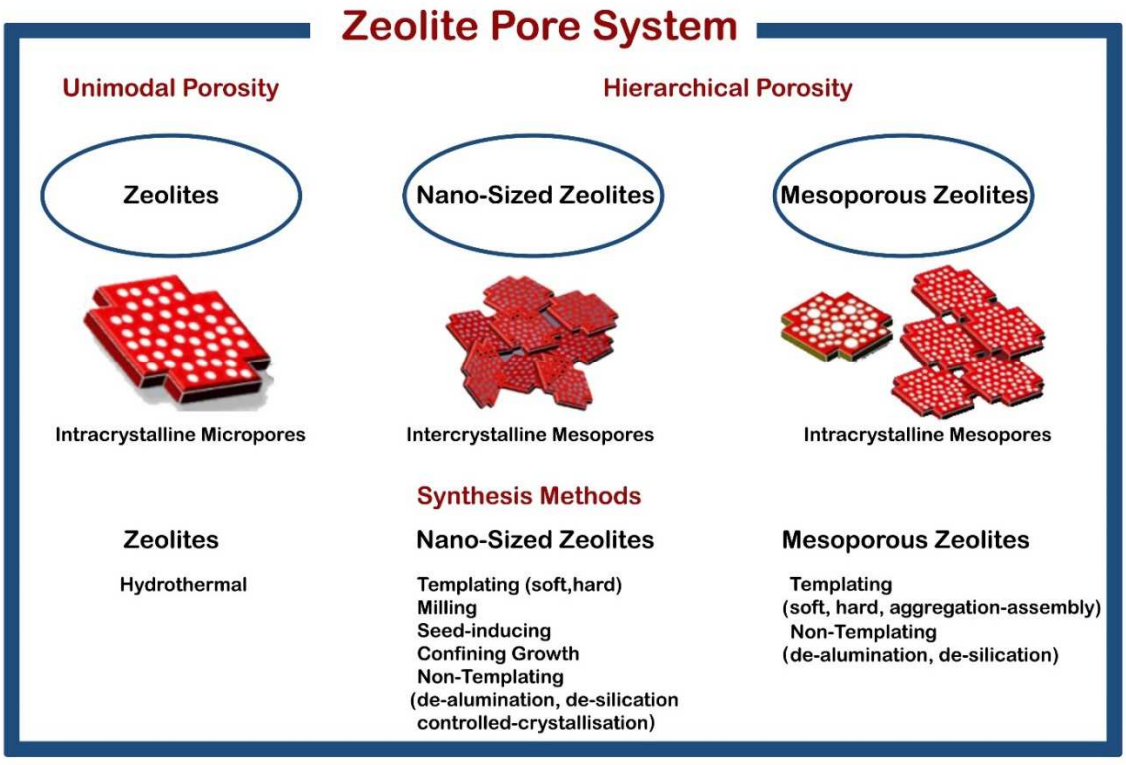

Figure 6. Zeolites' pore systems and synthesis techniques. Intra-figures reproduced with permission from [51]

In general, creating additional porosity at a larger scale in zeolites can be accomplished by either templating method or post-synthetic treatment (see Figure 6). The latter method includes de-alumination and de-silication which often leads to a partial collapse of the periodic zeolite structure, due to the difficulty in creating uniform mesopores with this method [52]. On the other hand, the use of mesoporous templates in the synthesis of zeolites enables more accurate control of the size of the mesopores, and these templates can be roughly classified as soft and hard templates [53]. Soft templates, such as surfactant micelles and silylated polymers, must keep a sufficient level of affinity with the zeolite framework so that separated phases won't be formed. On the other hand, hard templates, such as carbon materials, have reduced effect on the zeolite structure due to the weaker interaction with synthesis materials. This is indeed recommended for preserving the zeolites' high crystallinity. In addition, being present in different forms, the resulting mesoposority can be tailored by changing the form and properties of the carbon material used. In particular, carbon nanotubes (CNTs), having high aspect ratio and modifiable diameter, were efficiently used as hard-templates in hierarchical zeolite synthesis [52]. Depending on whether the zeolite particles were synthesized outside or inside the CNTs, an intra or inter-crystalline network of mesopores can be obtained, respectively. In Figure 6, hierarchical zeolite pore systems are classified and the corresponding synthesis methods for each classification are listed [51]. In addition, nano-sized zeolites can be synthesized by templating, milling, seed-inducing and confining growth methods [51]. Non-templating methods can also be utilized to synthesize nanozeolites, where the reaction is allowed to run under optimum conditions of temperature and type of precursor without using templates. The latter method has the advantage of being scalable and thus can be used for a wider range of applications. Seed-inducing method involves the addition of zeolite seeds to a synthetic gel and can produce high yield of the desired zeolite. For example, Lewis acidic nano-MFI zeolite was synthesized at low temperature conditions, resulting in five-fold reduction in particle size as compared to conventionally produced MFI via hydrothermal synthesis [54].

A mesoporous Y-zeolite was synthesized using a novel aggregation-assembly method where block copolymers were used as templates to direct the alumino-silicate gel to align forming mesoporous zeolite [55]. The synthesized zeolite consisted of two types of mesoporosities classified, according to their sizes, into small (6.5 nm) and large (35 nm) mesopores. The acidity of the synthesized zeolites was adjusted, in which the total number of acid sites decreased in the mesoporous samples, and the acidity strength (strong/weak acid ratio) decreased as well. It was reported that the mesoporosity in the catalyst facilitated the mass transport to the active sites, lowering the creation of coke and simultaneously increasing the yield of useful products. These results prove the significance of structural properties of the mesoporous zeolites in achieving high catalytic performance and activity.

Recent studies have shown that zeolite particle size and crystallinity has been actively controlled using the graphitic structure of graphene [56].The random orientation of zeolite nanocrystals templated on molecular assemblies result in an increase of surface area (520 m^2/g) and controlled porosity in the range of 2 to 20 nm [57]. Nanoporous zeolite-Y was synthesized using polyelectrolyte functionalized graphene oxide [58]. Graphene oxide nanosheet based assembly was utilized to synthesize zeolite-Y/GO composite, which was then purified into zeolite-Y by functionalizing the GO with cationic electrolyte.

Hierarchical zeolites having a densely interconnected network of micropores combined with meso- and/or macro-porous zeolites are interesting materials for hydrocracking as they tend to improve the selectivity and resist deactivation [59]. High FAU-content Faujasite nanocrystals with varying molar compositions were synthesized from organic-free sols in [60]. The effects of synthesis conditions on the content of FAU/EMT and the size of nanocrystals formed were both examined. The results confirm the precursor nanoparticle evolution and highlight the significance of solution composition at pre-nucleation and post-nucleation phases of aggregative crystal growth. A structural study has been performed on hierarchical zeolite X using TEM imaging and diffraction in [61]. The proposed conceptual model proves that the synthesized material is an intergrowth of FAU and EMT, where the growth of FAU occurs through a small percentage of EMT in an atypical morphology of assembled sheets with properly determined intersection angles.

An effective strategy for tailoring the structure and morphology of mesoporous zeolites is to introduce appropriate surfactants (i.e. soft templates) in the synthesis method. Figure 7 shows

SEM images of various hierarchical zeolites with different morphologies including nanosponge MFI zeolite (7A), multi-lamellar ZSM-5 (7B) and NaP zeolite with diamond (7C), cactus-like (7D) and wool ball-like (7E) morphology. The MFI zeolite nanosponges, shown in Figure 7A, were synthesized using the micropore-mesopore di-quaternary ammonium surfactant $C_{18}H_{37}$-$N^+(CH_3)_2$-C_6H_{12}-$N^+(CH_3)_2$-C_4H_9 in [62]. The mixture was converted through a dry-gel process, initially at 60^{o}C, to form a mesoporous material that resembles the MCM-41 structure. It was then filtered, dried and heated at 150^{o}C with monitored humidity and precursor pH to ensure complete zeolite crystallization. The resulting MFI zeolite consisted of 2.5 nm thick nanolayers arranged in 3D networks with high surface area and mesopore diameters of around 4 nm. It was observed that the original gel morphology was preserved during crystallization under monitored optimum chamber relative humidity of 80%, and optimum gel composition of 100 SiO_2/1 Al_2O_3/7.5 $C_{18\text{-}6\text{-}4}$/28.6 Na_2O/15 H_2SO_4/6000 H_2O. In comparison, at humidity levels as high as 100%, the sizes of the zeolite nanosponge particles were relatively large. It is worth mentioning that the synthesized dry-gel zeolite had comparable quality to that formed from conventional hydrothermal synthesis, with the advantage of remarkably reducing the autoclave size, thus allowing easier and faster large-scale synthesis.

Similarly, ZSM-5 zeolite with multi-lamellar structure, as shown in Figure 7B, was synthesized using dual-functional quaternary ammonium surfactant for high mesoporosity [63]. The synthesized zeolite exhibited higher surface area, larger volume of mesoporosity, increased catalytic lifetime, greater amount of active sites, and lower diffusion limitation, resulting in easier accessibility of acid sites. The catalytic performance results of the hierarchical MFI zeolite of thin nanosheets morphology suggested that improved mass transport and catalytic activity were associated with the given catalyst structure, in comparison to large crystal size MFI zeolite particles. The proposed zeolite synthesis method using the dual-functional surfactant provides guidance for potentially synthesizing various hierarchically-structured zeolites with tailored mesoporosity. On the other hand, hierarchical lamellar zeolites were synthesized using sequential intergrowth induced by the variation of synthetic gel composition [64]. Compared to classical approaches, a rather simple gel composition was used. The proposed composition lacked sulfate salts, particularly sodium sulfate, and limited the amount of di-quaternary ammonium surfactant template used. The results showed that mesoporosity of the product increases with higher content

of ammonium surfactant, but stays rather constant with the change in Si/Al ratio of the starting materials.

ZSM-5 zeolite in different particle sizes, and in the form of nanosheets were also synthesized in [56], [65]. The experimental conditions were varied to obtain uni-lamellar and multi-lamellar zeolite sheets; for further information on these conditions, the reader is referred to [56]. In both nanosheet zeolite preparation methods, a bromide form of the surfactant was used. In contrast to the findings of [63], the zeolite nanosheets had considerably lower inner surface area and path lengths of the micropores when compared to the zeolite particles, implying potentially decreased contact between the reactants and the acid sites of the catalyst which caused its lower catalytic activity in cracking n-heptane [65].

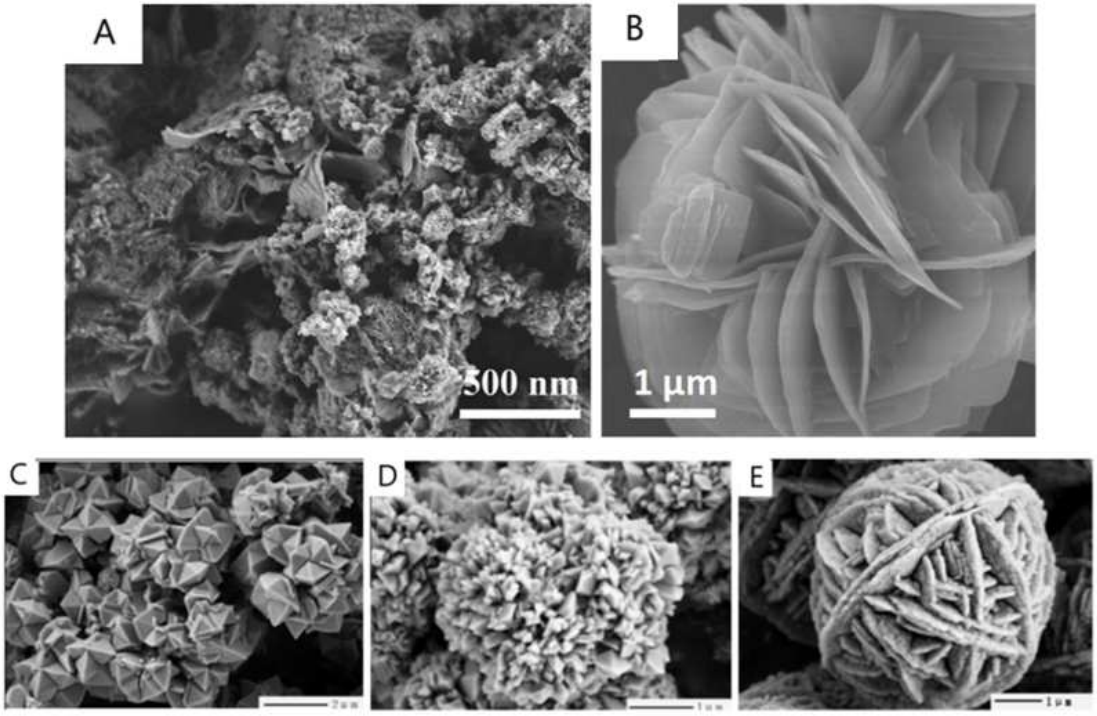

Figure 7. Various zeolite morphologies: (A) nanosponge MFI zeolite [62], (B) multi-lamellar ZSM-5 zeolite [63], (C) diamond morphology (D) cactus-like morphology, and (E) wool ball-like morphology of zeolite NaP [66]. Reproduced with permission from [62], [63], [66]

In a different study, nano-sponge beta zeolite was prepared using a surfactant of a meso-micro hierarchical structure, resulting in 10-20 nm thick interconnected nanocrystals [67]. The nano-sponge morphology of the zeolite involved large surface area and even mesopores leading to high accessibility of active acid sites and relatively easy diffusion of reactants and products via the mesopores. Figure 8A and 8B represent SEM and HR-TEM images, respectively, of the nano-sponge beta zeolite with Si/Al ratio of 110, and Figure 8C presents an SEM image of a conventional beta zeolite of Si/Al ratio of 103 [67]. Figure 8A indicates that the synthesized zeolite consists of thin nanocrystals of approximately 10-20 nm, that are arbitrary interconnected to produce a nanosponge-like assembly, with no clear additional phases. As shown in Figure 8C, the conventional beta zeolite composed of aggregates, in the range of 500 to 1000 nm, of the particles with a diameter range of 30-50 nm.

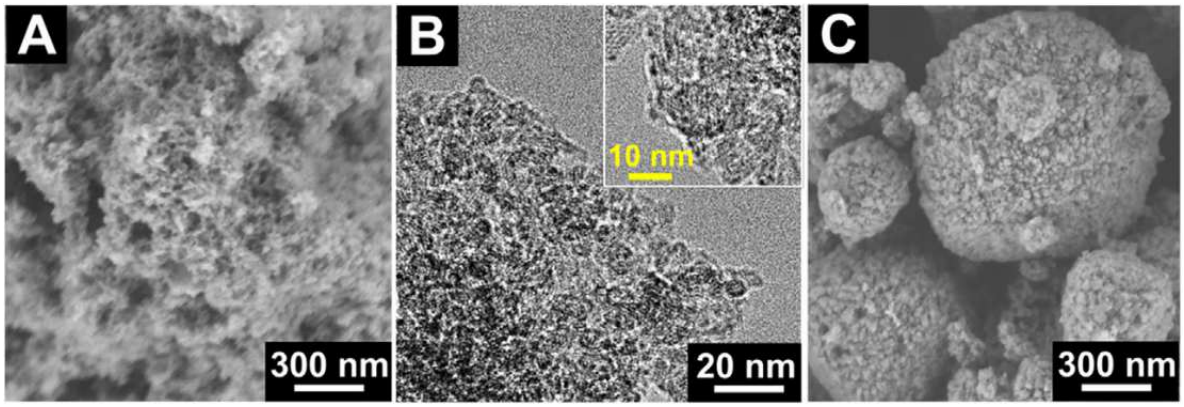

Figure 8. SEM (A) and HR-TEM (B) images of nanosponge zeolite (Si/Al=110), SEM image (C) of conventional zeolite (Si/Al=103). Reproduced with permission from [67]

Other authors synthesized a Co-based composite zeolite, MOR/ZSM-5, using a solvent-free synthesis recipe for several crystallization periods [68]. Different morphologies were observed for different crystallization times, with the optimal time being 72 hours of crystallization at which perfect crystal structure was obtained.

Moreover, a hydrocracking catalyst carrier made of amorphous binder and zeolite Y of Si/Al ratio of 10 was patented in [69]. The uniqueness of the patented support is due to the calcination step performed at high but narrow range of temperatures; between 700 to 900^{o}C, after which loss of

zeolite crystallinity occurs. The optimal calcination duration was found to be between 30 minutes to 4 hours, at ambient pressure in air.

The synthesis of CNT/zeolite hybrid catalyst often involves the growth of one of the components on the other. For instance, CNTs were grown on a mixture of zeolite and Co precursor by methane decomposition, in a process similar to chemical vapour deposition (CVD) [70]. Calcination in air, reduction in hydrogen, and then methane decomposition were carried out consecutively at various temperatures (300 to 500^{o}C) and for different durations (15 to 60 min). It was realized that when the calcination temperature or time was decreased smaller quantity of the metal was formed and thus CNT formation decreased. Also, reducing the reduction temperature favoured the formation of smaller metal particles, and thus CNTs with smaller diameters were produced causing lower carbon content in the final catalyst. However, given that CNTs will grow on the Co metal in catalytic reactions where the exposure of Co particles is necessary, this method would rather need modifications. Alternatively, the zeolite can be allowed to grow on CNTs by modifying the hydrothermal method of zeolite synthesis. It was proposed in [71] to add previously treated and sonicated CNTs into fumed silica and sodium hydroxide solution before the addition of the mixture to a separately prepared sodium aluminate solution. The typical hydrothermal method is then used to grow sodium zeolite Y on the CNTs to obtain the composite catalyst, Na-ZY/CNT. Although this method was successful, SEM images showed that the CNTs were not uniformly dispersed in the composite, limiting the periodicity of the mesopores formed by the CNTs [71].

One method for tuning the zeolite properties is by varying the template molecules such that to control the distribution of Al atoms within the zeolite framework. According to the *Löwenstein rule*, the formation of Al-O-Al linkages is prohibited within the zeolite framework, even though it was proposed that some violations to this rule are theoretically possible [72]. Yet, even without breaking this rule, the presence of Al in Al-O-Si-O-Al or Al-O-(Si-O)$_n$-Al (n=2,3) is crucial for the catalytic properties and for stabilizing the transition metal cations. For example, a pair of Al atoms close to each other can balance the charge of a divalent cation, while an isolated Al atom cannot [72].

2.2 Metal loading on acid supports

Metal particles catalyse both hydrogenation and dehydrogenation reactions in hydrocracking processes and are typically supported by the microporous or mesoporous zeolite. Various

combinations of metal particles have been tested and presented in the literature, and it has been shown that the catalytic activity and selectivity are often improved by placing the metal as close as possible to the acid sites on the supports of the bi-functional catalyst [73]. The latter condition can be achieved by synthesizing nano-sized metal particles, thus increasing the contact area between the metal and the support and facilitating the spillover and back-spillover of species in the hydrocarbon reactions [74]–[77]. The optimal catalyst activity is reached through maximizing active sites density, while preserving the access required for the feed molecules [78].

Metal loading on the acid support is often done through metal impregnation or co-impregnation. Metal precursors in the form of salts (e.g. metal nitrates) are dissolved in deionized water in order to prepare solutions with predetermined metal quantity. The solution is then stirred and added to the previously prepared support. After absorbing the metal, the catalyst is then dried and finally calcined [79].

Various factors contribute to the chemistry of impregnation. The pH, for instance, is a significant parameter in the impregnation process due to the presence of a mixture of acidic and basic species in the solution subjected to various pH-dependant reactions of association and dissociation until the equilibrium point. Furthermore, the pH determines the sign of the global surface charge and the amount of charge sites on the solid side, and affects, both thermodynamically and kinetically, the dissolution of the oxide support [80]. An appropriate selection of pH would facilitate the deposition of the most abundant species in the solution to the support. HNO_3, carboxylic acids or NH_3 are convenient choices as pH adjusters since they can be easily removed post-synthetically with thermal treatments. As for incipient wetness impregnation, the pH is regulated by acido-basic surface hydroxyls of the support, known as *buffer effect*, since the solutions are neither very acidic nor very basic. However, pH control inside the pore system is still challenging particularly for non-equilibrium conditions, such as in the cases where the composition of the solution is non-uniform inside the pellet. In addition to the pH of the solution, precursor-support interactions are also important parameters for the study of active phase dispersion. For low precursor concentration, the interactions between metal ions and oxide surface are the driving force for individual metal ion adsorption, whereas for high precursor concentration, the interacting species with the surface act as seeds for the salt crystallization upon drying [80]. The main interactions between the chemical species during the process of impregnation and drying can be described by

adsorption (from electrostatic interactions to grafting), and the formation of mixed phases; for further details, the reader is referred to the literature [80].

Electrostatic adsorption is an adsorption mechanism at the molecular level in which charged species adsorb into an oxide support from an aqueous solution. In other words, solid surfaces tend to acquire electrical charge when contacting an aqueous phase creating a microenvironment of electrical potential imbalance at the solution-surface interface, affecting the distribution of the surrounding ions [81]. Various hydrous metal oxides and organic compounds comprise ionisable functional groups at their surfaces that might disassociate developing surface charge (e.g. OH groups). In order to preserve electro-neutrality, the total net charge of the support surface and the solution must be balanced from a macroscopic perspective, leading to what is called point of zero charge (PZC). The surface charge depends in the first place on the *pH* of the surrounding solution. The fact that amphoteric surface groups exist on the surface of oxides can allow electrostatic adsorption of anions at low pH values and cations at high pH values for the same support [82]. This is because, in alkaline mediums, the net charge on the surface is negative, while under acidic conditions, excess protons are held by the surface resulting in a net positive charge [81]. Beside the pH, other factors can also affect the electrostatic adsorption. *Temperature*, for example, has an effect on the surface charge of the adsorbent material and thus, its point of zero charge. Additionally, metal complexation by organic ligands with more than one functional group typically improves metal adsorption as the other functional groups bond to the solid surface, indicating an effect of the *solute speciation* on the electrostatic adsorption process [81].

The double layer theory shall be utilized to formulate the electrostatic adsorption, in which the first layer represents the support surface, being positively or negatively charged based on whether it is protonated or deprotonated, while the second layer is the region of the solution where the electrostatic potential created by the surface charge significantly affects the ion concentrations [82]. The double layer model is illustrated in Figure 9 (a), and an example of the three possible scenarios for solution pH (relative to PZC) and type of charge adsorbed is shown in Figure 9 (b).

The electric potential of a surface's slipping plane relative to the bulk solution created in a double layer, also known as zeta potential, is used to quantify the charge magnitude. Zeta potential curves for zeolites normally drop down with an increase in the *pH of the medium*, and the *temperature* [83].

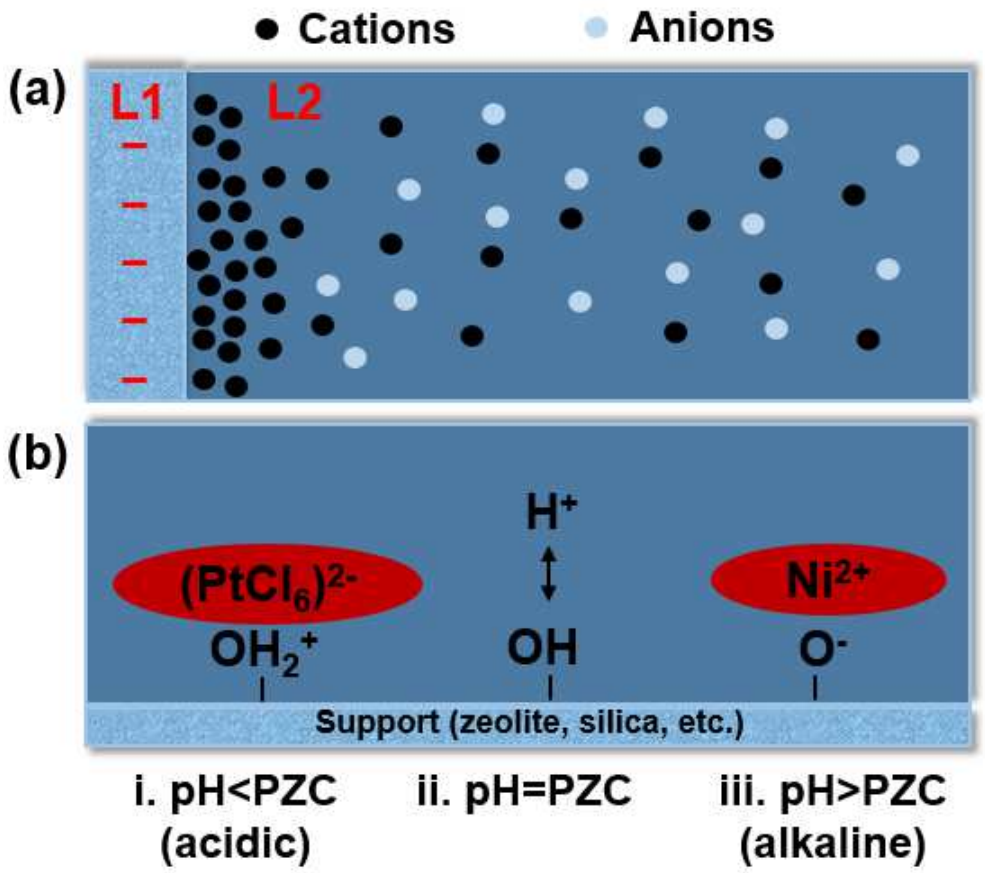

483

484 **Figure 9.** Double layer model representing electrostatic adsorption of (a) cations from an
485 aqueous solution layer (L2) on a negatively charged support layer (L1), and (b) three possible
486 adsorption scenarios (i, ii, and iii) based on the solution pH

487 Memory effects are claimed to exist in the synthesis of supported catalysts, in which the system
488 may remember for a long time the preparation conditions initially applied. Although this claim is
489 still not very well established, one can rely on specific cases and examples in which these effects
490 hold. In these cases, controlled changes in the metal deposition mechanism translates into
491 variations in the final catalyst, and thus unified recipes for the catalyst preparation have to be
492 followed each time the same catalyst is to be synthesized [82]. For instance, in the preparation of
493 the bimetallic system, $[PtCl_6]^{-2}WO_xAl_2O_3$, the alumina surface is first modified by tungstate
494 deposition after which washing, drying, chloroplatinate deposition, drying again and thermal
495 treatments are carried out [82]. During these preparation steps, the sequence of events happening
496 was found to highly depend on the nature of the tungstate salt, initially used for deposition, and on
497 the deposition mechanism. Monotungstate $(WO_4)^{-2}$ was deposited in small quantities by an *inner-*

sphere mechanism, while Paratungstate $(H_2W_{12}O_{42})^{-10}$ followed specific adsorption as *outer-sphere* complexes with charge overcompensation. Metatungstate $(H_2W_{12}O_{40})^{-6}$ was generally electrostatically adsorbed and stayed mobile on the surface. Inner-sphere mechanism is one in which a bridging ligand is formed to transfer electrons between complexes involving breakdown and formation of bonds. Outer sphere, on the contrary, is an electron transfer mechanism between complexes that do not undergo substitution and involves no bond breakdown or formation.

Alternatively, metal-supported catalysts can be prepared by the deposition-precipitation (DP) method. The success of this method relies on several parameters that need to be pre-determined, such as temperature, stirring rate, synthesis duration (DP time), concentration of the support, urea, and nitic acid [84]. The standard DP method involves the use of excess amount of the metal precursor and then changes the DP time in order to regulate the amount of metal loading. Instead, the starting metal precursor concentration can be selected in such a manner to control the metal loading, and the DP duration can then be set for an excess time [85]. Generally, a solution of the metal precursor with pre-determined concentration is first prepared. The support (e.g. zeolite) is then added to the majority (around 4/5) of the metal solution, and the slurry formed is heated to 70^{o}C under agitation. Then, urea and nitric acid are added to the remaining metal solution forming a new solution that is consequently added dropwise to the heated slurry. Next, the temperature is increased to 90^{o}C and kept for as long as the desired DP time with continuous stirring. Finally, the slurry is quenched in an ice bath, vacuum filtered, washed with deionized water, dried overnight, and calcined.

Remarkable thermal stability has been shown for silica supported metal catalysts prepared by DP as compared to their impregnation counterparts [86]. The urea DP method has been most widely used to prepare supported Ni-catalysts, but a range of other metals have been successfully deposited by this method. Copper deposition on silica using urea, however, has been exceptionally challenging especially with the use of copper nitrate precursor, $Cu_2(NO_3)(OH)_3$, which precipitates at pH of 5 when the interaction with the silica support is poor [86]. Extended precipitation time is required in such case to dissolve the basic copper nitrate and precipitate another copper compound at elevated pH having good interaction with the support at which time copper hydro-silicate is formed. Although in divalent transition metals hydrolysis takes place at very low pH values preventing proper interaction with silica, typically favoured at pH>5, these metals can generally

be deposited using urea DP [86]. For instance, La(III)oxide was successfully deposited onto silica by adding NH_4OH solution starting with pH of 4 which was gradually increased until 10 in [87]. The results revealed an interaction between $La(OH)_3$ and SiO_2, whereas the XRD results showed that the La phase was amorphous.

Another method for metal loading would be to encapsulate the metal in the support structure *in situ* during the support synthesis [88]. For zeolite supports, an alumina-silicate gel is prepared in the desired composition, and an aqueous solution of the metal precursor is added to the gel, at 60^oC, dropwise with continuous stirring for 1 hour. After that, the conventional procedure for the zeolite synthesis is followed. Whether *in situ* or as post-synthesis modification, once the active phase is dispersed inside the zeolite, the zeolite framework protects the metal from sintering even at increased temperatures [72]. Such an approach was employed to synthesize Pt nano-particulates supported on ZSM-5 *nano-shells* having extremely thin walls [89]. The Pt nanoparticles having diameters of 2-3 nm were entrapped and highly dispersed in the zeolite nanoshells, which resulted in high thermal stability up to 750^oC owing to their immobilization.

Based on the details of the synthesis method, various configurations of the metal-zeolite composites can be obtained, each having specific chemical, physical and catalytic properties. *Isolated metal nanoparticles*, *ion-exchanged cations* (stabilized in the $[AlO_4]^-$ tetrahedra), and *single heteroatoms* substituted in the zeolite framework are three conceptually different transition metal-zeolite composites schematically illustrated in Figure 10. Well-defined *single-atom catalysts* can be prepared by chemical vapour deposition (CVD) method, in which a volatile and reactive metal precursor is allowed to react with a zeolite under anhydrous conditions and elevated temperatures [72].

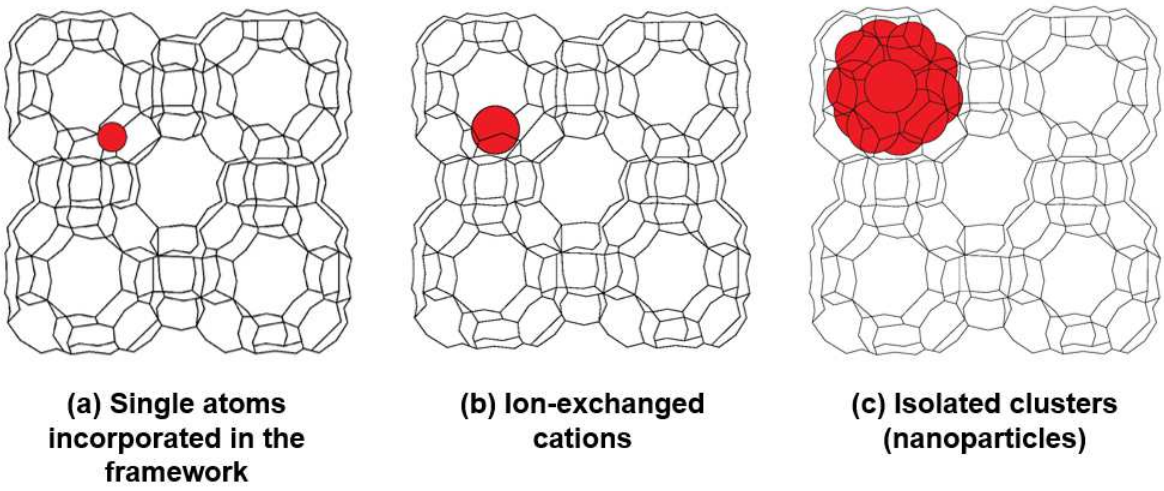

550

551 **Figure 10.** Metal-zeolite composites in three possible configurations: (a) single heteroatoms, (b)
552 ion-exchanged cations, (c) isolated metal nanoparticles

553

554 For hydrocracking of heavy oil, Molybdenum and Tungsten sulfides are used as active species in
555 metal-supported catalysts with Ni and Co being the promoting species [90]. These active species
556 are then dispersed on an acid support, such as alumina [57], [91], alumino-silicates [92], [93] or
557 zeolites. Despite being efficient catalysts for hydrocracking, these metal-supported catalysts are
558 also used for hydro-desulfurization (HDS) [94] and hydro-demetallation (HDM) processes [95].
559 However, metal supported materials are unfavourable catalysts for hydrocracking extra-heavy oil,
560 due to rapid coke and sulfur formation on active sites, which in turn causes catalyst deactivation
561 [96]. Instead, un-supported, highly dispersed metal catalysts are rather used for extra-heavy oil
562 hydrocracking such as nickel or cobalt molybdenum sulfides [97]–[102].

563 A novel hydrocracking catalyst and preparation method comprising a support, an active metal and
564 carbon is patented [103]. With respect to the total weight of the catalyst, the support is present in
565 60-90 wt%, while the active metal component in metal oxide is 15-40 wt%, and the carbon element
566 is 1-5 wt%. The steps involved in this innovative synthesis are: (i) carbon deposition reaction to
567 obtain a carbonized support by allowing the support to be in contact with a carbon source; (ii)
568 treating the carbonized support in an oxygen-containing gas (0.5-8 vol%) at 250°C-390°C in order
569 to obtain a decarbonized support of carbon content between 20-80% of that in carbonized support;

(iii) introduce the active metal precursor into the decarbonized support and allow to dry; (iv) heat treatment to convert the precursor into active metal oxide, while keeping the carbon in the support.

Recently, various research groups reported the formation of unique metal oxide architectures; nanosheets [104], nanoflakes [105], nanoplates [106], flower like nanoparticles [101], [107], [108] and porous nanoparticles [109], on CNT/graphene templates as shown in Figure 11. These types of particles have enhanced porosity and surface area as compared to particles of nearly spherical shape, but their performance in hydrocracking applications has yet to be proven.

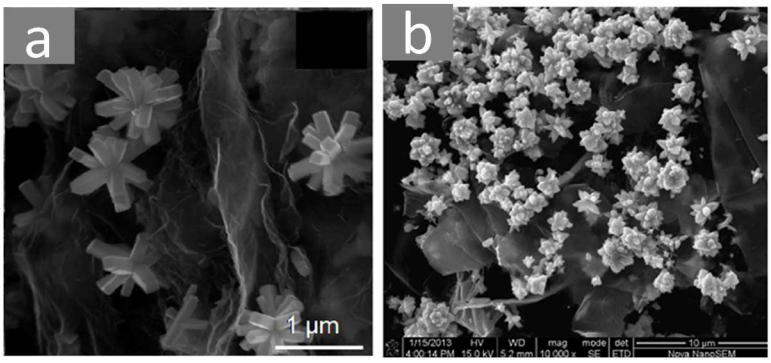

Figure 11. Scanning electron microscopy (SEM) image of (a) flower-like SnO_2/graphene [108] (b) flower-like ZnO/RGO composites [110]

2.3 Pelletized catalysts for industrial use

Matrix materials or binders (e.g. clays, aluminas and silicas) are often used in industrial applications to disperse the catalyst into desired formable shapes (e.g. granules, trilobes, cylinders, rings, etc.) enhancing their mechanical and attrition resistance [111]. They are particularly used when the stability and mechanical strength of the catalyst need to be improved for certain reaction conditions. Although catalysts in fundamental studies are often carried out in powder form for simplicity, industrially-used catalysts involve the preparation of pelletized-catalysts including the active components of the catalyst and a binder. Thus, it is important to highlight the preparation methods for pellets and their effect on hydrocracking reactions.

2.3.1 Pellet preparation

Mulling-extrusion method is the most commonly used shaping method for zeolites, in which the binder used is typically alumina or silica as shaped zeolites possess poor mechanical resistance [112]. The preparation steps briefly involve mixing of zeolite, binder, and methylcellulose (organic binder) powders in an aqueous solution of nitric acid, kneading the mixture and adding an aqueous solution of ammonium, extruding the paste, and finally drying and calcining the extrudates [112], [113]. The metals can later be deposited on the shaped zeolite following simple impregnation method. Moreover, pelletization of zeolites can be done by agglomeration, in which materials with good binding properties, such as the sodium form of bentonite clay, can be utilized for this preparation technique. Simply, the zeolite and bentonite are suspended in water with mild heating and continuous agitation, then dried, and later grinded and sieved (to collect the particles of desired size), before being calcined [114]. However, in this method further processing is required to obtain the acid-form of the agglomerated zeolite, which can be achieved by ion-exchanging Na^+ several times with NH_4Cl under agitation at mild temperature followed by calcination. Finally, the metals can be incorporated in the catalyst by impregnation method [115]. Also, extrudates preparation has been reported with controlled deposition of platinum by changing the sequence of the preparation steps: Pt impregnation on the zeolite, catalyst synthesis, and catalyst shaping [116]. The study indicated that the alternative ways of Pt deposition on the extrudates had significant effects on the metal-to-acid site ratio; the binder presence reduced the acidic properties of the zeolite due to changes in the solid-state ion exchange between zeolite protons and clay sodium. Also, the morphology, metal particle size, total acidity, and mechanical strength of the shaped catalysts were highly affected by the preparation method adopted. The study showed that the strength of the extrudate increased with increasing Pt concentration, and that Pt particle size was reduced in all types of extrudate due to extrusion [116]. Thus, the mechanical strength of the extrudates depends on the binder type, ratio of the support and the binder used for preparation, the particle size and the calcination step.

From the aforementioned, it would be beneficial to shed more light on metal-loading of pellets at a molecular-level. The conditions applied during the impregnation and drying steps, and the type of competitor molecules (i.e. molecules that enhance the metal distribution) introduced in the impregnation, lead to various ways of precursor distribution on the support, namely egg-shell, uniform, and egg-yolk distributions, as shown in Figure 12 [80]. Egg-shell distribution (Figure

12a) can be obtained when a highly viscous solution of the precursor is used during impregnation leading to strong adsorption of the precursor. The same distribution can also be obtained in the case of low viscosity solutions if slow drying regime is adopted. When equal competition exists between the precursor and competitor with the support surface, a rather uniform distribution (Figure 12b) occurs. Uniform distribution can also be the result of weakly interacting precursor accompanied with room temperature drying. In contrast, egg-yolk distribution takes place when the competitor interacts more strongly with the surface as compared to the precursor favouring the diffusion of precursor solute towards the center of the pellet, or when fast drying regime is applied with predominant back-diffusion [80]. For instance, Eggshell and uniformly distributed Pt catalysts were prepared via the post synthesis and in-situ synthesis methods, respectively [116]. The post synthesis method in this context refers to the impregnation of Pt on the extrudates after shaping by extrusion, whereas in-situ synthesis involves Pt impregnation prior to shaping and extrusion, i.e. Pt deposition on the zeolite and/or binder. Intimacy effects for metal-mesoporous solid acids catalysts were studied by preparing mesoporous supports with or without binders. For further information the reader is referred to [117].

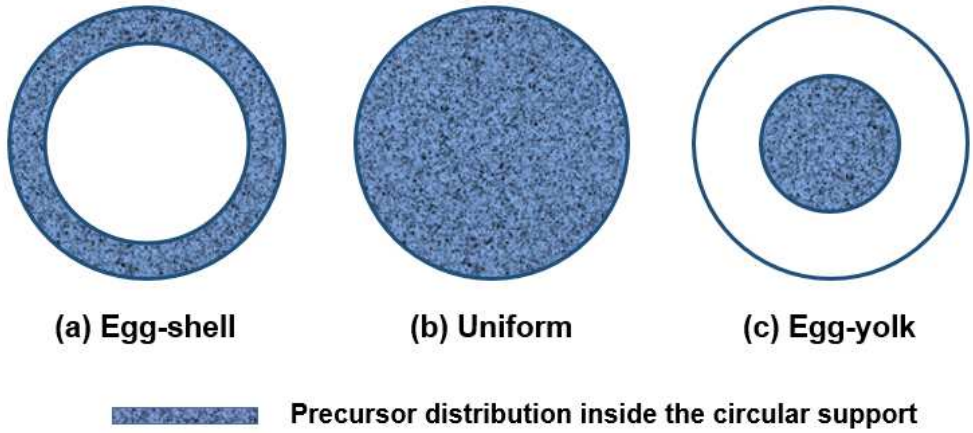

Figure 12. Types of possible metal precursor distribution during the wetness impregnation method of catalysts preparation

2.3.2 Binder's effect on catalyst properties

Even though they might be seen as inert components, binders can have substantial effect on the catalyst performance in hydrocracking. The major effects of the binder on the catalyst properties and performance are summarized as follows [111].

Alteration of the catalyst porosity: The presence of an additional phase in a catalyst is clearly expected to modify its porosity and thus causes certain changes in the reaction performance. Binders were reported in some studies to induce meso- or macro- porosity to the zeolites causing beneficial selectivity effects attributed to improved diffusion as metals disperse into the meso- or macro- pores of the binder [111]. The development and application of hierarchical zeolites in large-scale industrial processes typically involve binders and this was considered in a number of studies [118], [119]. The main observations in these studies were that mesoporosity was generated in the zeolite-binder catalyst arising from the inter-crystalline voids of alumina crystallites [118]. Although this improved the performance of the catalyst, it reduced the dispersion of metal too, and therefore, optimizing the binder percentage in the catalyst becomes necessary. Similar findings were reported in [119] where the presence of the binder increased the mesopore volume and the average pore volume, whereas the micropore volume and the surface area were both reduced.

Alteration of the catalyst's coking resistance: Several studies demonstrated that coking was reduced with the addition of a binder to the catalyst since coke precursors were trapped by the binder. For example, the stability of de-aluminated mordenite catalyst in converting methanol to light olefins significantly increased with the addition of a binder due to the trapping of coke precursors by the binder [111]. Investigating the pure phases showed that coke accumulation on the zeolite decreased while that on the binder increased. In contrast, the presence of the binder caused a reduction in the catalyst activity, and acidity, as the strongest proton sites were neutralized by alkaline earth metals coming from the binder during the catalyst synthesis. Yet, not all studies involving binders reported a reduction in coke level with the presence of binders, but rather correlated coking level with the nature of the binder used. Alumina binders resulted in an increase in the coke deposition on the zeolite phase, kaolin binders did not cause noticeable change, whereas silica binders decreased the deactivation caused by coking due to a simultaneous decrease in external and intra-crystalline acidity of the zeolite [111].

Trapping poisons: The presence of metal components in hydrocracking feedstock is a well-known problem that leads to poisoning and possibly catalyst deactivation. The presence of binders, fillers and matrices has been shown to somehow mitigate the effect of metal presence in the feed and enhance the tolerance of the catalysts [111]. For example, the presence of a basic compound, such as magnesia in magnesia-alumina matrix, can trap H_3VO_4 protecting the zeolite from the effect of vanadium.

Altering the thermal characteristics of the catalyst: Although minimal experimental validation has been carried out, it has been reported that binders can act as heat sinks in exothermic reactions. This potential characteristic of the binders may be beneficial for regulating the reaction conversion and/or selectivity with the possibility of preserving the integrity of catalytically active phases, such as by reducing sintering [111].

Enhancement of physical durability: One of the main advantages of adding binders is to improve the mechanical strength of the catalysts by shaping them into different forms including granules, pellets, extrudes and monoliths, depending on the desired application. Based on the degree of the thermal treatment and thus, the dehydration of the binder during synthesis, terminal hydroxyl group cross-linking is induced, leading to an increase in the mechanical strength of the catalyst [111].

3. Performance of hydrocracking catalysts

A large body of literature now exists that demonstrates the effectiveness of zeolite-based bi-functional catalysts in hydrocracking of a wide variety of feedstocks. In order to maximize the process performance, it is paramount to tailor the composition, structure, morphology, acidity and porosity of the catalyst to the process conditions and structure of the feed molecules. The process conditions indeed play an important role on the performance of a hydrocracking process. An increase in temperature typically results in faster cracking on acid sites, yet, very high temperatures limit the hydrocracking of aromatic compounds. Increasing the hydrogen partial pressure increases the conversion of aromatics into saturated products, thus, enhancing the quality of jet and diesel fuels with remarkably high viscosity index [120]. Hydrocracking aromatic hydrocarbons is

optimally performed at high pressure and hydrogen to feed ratio, combined with the lowest possible temperature.

The evaluation of a catalyst performance in cracking processes is commonly based on a number of reaction metrics. The conversion is the number of moles of a reactant that has been transformed into products over the number of moles of that reactant fed, and can be expressed as

$$X = \frac{number\ of\ reacted\ moles\ of a\ reactant}{number\ of\ introduced\ moles\ of\ that\ reactant}\ x\ 100\ . \quad (10)$$

When new catalysts are developed, conversion is typically the first parameter to be measured [121]. In complex reactions, conversion alone is insufficient for describing the catalyst performance, and properties such as selectivity and yield need to be measured too. Selectivity is the amount of certain product formed during the reaction; generally, it is defined as the number of moles of a product formed over the number of moles of reactants converted to form the product:

$$S = \frac{number\ of\ moles\ of a\ desired\ product\ formed}{number\ of\ moles\ of\ all\ products\ formed}\ x\ 100\ . \quad (11)$$

However, the definitions for selectivity take different forms, and thus, precise definition is required when reporting selectivity of a catalyst. Based on these definitions, it can be deduced that selectivity depends on conversion, and although high selectivity of the desired product is favorable, it is also desirable to achieve large enough reactant conversion. Therefore, a third characteristic property, known as the yield, is often essential for catalyst evaluation. Yield, often measured in percentage weight, is the ratio between number of moles of a product of interest and the number of moles of reactants fed, and can be calculated through the following formula:

$$Y = \frac{no.of\ moles\ of\ a\ desired\ product\ formed\ from\ reacted\ moles\ of\ i}{no.of\ introduced\ moles\ of\ i}\ x\ 100\ . \quad (12)$$

The challenge is to maximize the yield of the desired product through the use of highly active catalysts that can facilitate high conversion rates. Optimum catalyst selection will certainly depend on the required outcomes for the specific application of interest [122].

Apart from the metrics described above, catalyst lifetime is also an important consideration. Catalyst deactivation deteriorates the aforementioned functional properties during the reaction. In

case of hydrocracking, the lifetime of a catalyst can vary from a few seconds up to a few years. Several factors may contribute to catalyst deactivation, such as poisoning, coke formation, and solid state transformations. Poisoning is often caused by chemisorption of impurities on the catalyst, while coking results from the carbon formation and deposition on the catalyst. Carbon can be formed as a product or intermediate product resulting from side reactions, in either case blocking the active sites. Solid state transformation, however, may involve a number of possible phenomena, such as carrier modification or promoter atoms' migration [121]. Both coke formation and poisoning by heavy metals lead to catalyst deactivation during hydrocracking which may or may not be reversible. Reversible deactivation arises from coke deposition and can therefore be retreated by burning coke in the generator. On the other hand, irreversible deactivation takes place due to four distinct but interconnected phenomena: zeolite de-alumination, zeolite decomposition, matrix surface collapse and metal (such as sodium and vanadium) contamination [40]. Protonic zeolites with high Si/Al ratio are considered stable, and prevent easy de-alumination. The most problematic metallic contamination is iron carried in with the feed, which might be suspended or combined with a molecule of heavy hydrocarbon. In both cases, such form of contamination does not only cause catalyst deactivation, but more critically, plugs the catalyst cavities resulting in considerable pressure drop [123]. Furthermore, other factors may also facilitate the deterioration of hydrocracking catalysts. For instance, increasing feed rate and conversion, as well as decreasing hydrogen partial pressure, reactor pressure, recycle gas rate and recycle gas purity all contribute to reducing the life of the catalyst. The activity of the hydrocracking catalyst diminishes with time, so in order to keep the design conversion rate, the catalyst temperature has to be increased. Accordingly, catalyst manufacturers specify an 'end of run' temperature (EOR) corresponding to the maximum temperature the catalyst can withstand, after which regeneration or discarding of the catalyst should take place [123].

In the following sections, we provide a detailed review of recent literature concerned with the design and performance evaluation of bi-functional catalysts in hydrocracking of a variety of feeds, including aromatic compounds, heavy petrochemical feedstock, paraffinic hydrocarbons, and vegetable oil. For each of these feeds we present, in the following sections, tables with references

to relevant studies which are meant to help the reader to identify common catalysts and products obtained from a particular type of feed.

3.1 Hydrocracking of aromatic compounds

We proceed to examine the current literature for information related to the performance of metal promoted zeolite-based catalysts in hydrocracking of aromatic compounds.

The effect of the zeolite's particle size on hydrocracking of 1-methylnaphthalene into benzene, toluene, and xylene (BTX) was demonstrated in [124]. In the latter study, nano-sized β zeolite (β-N) and micometer-sized β zeolite (β-M) were synthesized and loaded with Ni_2P for catalytic conversion of the naphthalene feed into BTX. The yields of BTX from the two hydrocracking processes were 42.3% and 30.5% for Ni_2P/β-N and Ni_2P/β-M, respectively. The use of nano-scale crystal size zeolite catalyst not only resulted in higher yield of BTX, but also demonstrated enhanced local and bulk structure stability and catalytic activity over the micro-sized crystal zeolite. TEM images for fresh and spent catalysts Ni_2P/β-N and Ni_2P/β-M are shown in Figure 13. The images clearly depict a variety of crystallite sizes, 20 nm for β-N and 0.5 μm for β-M. The Ni_2P particles were smaller in Ni_2P/β-N falling in the size range of 5–10 nm. In contrast, larger Ni_2P particles were found in Ni_2P/β-M of 10–50 nm size on the support. In addition, superior Ni_2P dispersion, and higher accessibility to acid sites in Ni_2P/β-N were enabled by the presence of inter-crystalline mesopores, subsequently facilitating the arrival of feed molecules to active cracking sites. In contrast, the hydrocracking over Ni_2P/β-M catalyst suffered from the production of coke, and had an overall poorer activity for both the hydrogenation and hydrocracking processes.

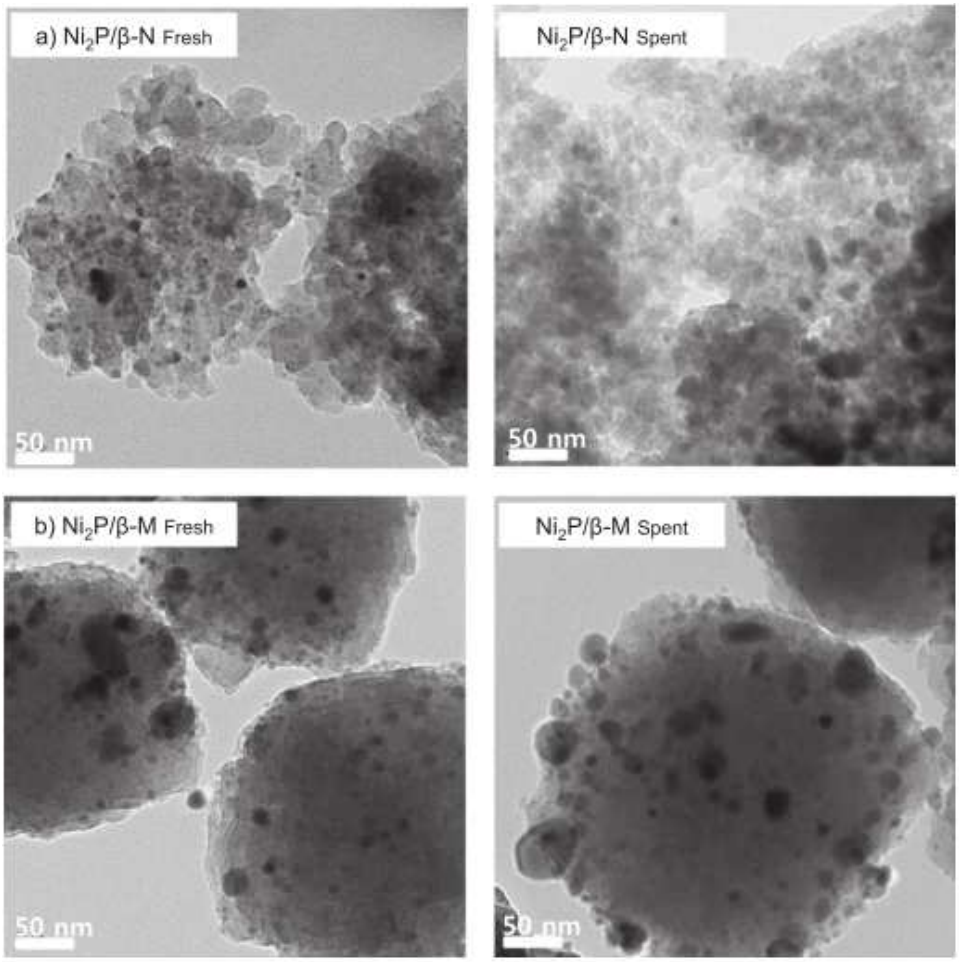

Figure 13. TEM images for fresh and spent catalysts Ni_2P/β-N and Ni_2P/β-M. Reproduced with permission from [124]

The performance of the catalytic conversion of naphthalene feeds into BTX not only depends on the catalyst's particle size but also on the details of the zeolite structure. This was shown in [125] where three types of zeolites, namely ZSM-5, β and USY were loaded with Ni_2P and used for catalytic hydrocracking of naphthalene into BTX [125]. In terms of catalytic activity, the Ni_2P/β catalyst was the best among those tested, exhibiting naphthalene conversion of 99%, and BTX yield of 94.4%. The improvement observed from the use of the latter catalyst was attributed to the proper dispersion of Ni_2P particles, and to the reasonable acidity and porosity of β zeolite. It is worth mentioning that EXAFS and XRD results proved that the stability of the Ni_2P/β catalyst was maintained during the cracking process. On the other hand, loading SiO_2, rather than zeolites, with

784 Ni_2P resulted in limited catalytic activity, and produced tetralin and decalin at 400°C and 30 bar
785 from the hydrogenation of naphthalene.

786 Different types of catalyst compositions were studied in [126] where Cr_2O_3 was introduced in
787 different amounts to Pt/ZrO_2 catalyst forming Pt/Cr_2O_3-ZrO_2. The obtained composite catalyst was
788 used for hydrocracking isopropylbenzene (IPB), 1,4-diisopropylbenzene (DIPB) and 1,3,5-
789 triisopropylbenzene (TIPB). The results indicated that by adding Cr_2O_3 to ZrO_2 the tetragonal
790 phase of ZrO_2 and the bulk crystalline Cr_2O_3 were strengthened. Additionally, the acidity and
791 surface area were both maximized for 8 wt% introduction of Cr_2O_3 but declined to some extent for
792 12 wt%. In particular, the Brønsted acid site concentration slightly decreased for the 12 wt% Cr_2O_3
793 loading, whereas the Lewis acid site concentration continued to increase with the Cr_2O_3 loading.
794 Based on the FTIR results, the 8 wt% loaded catalyst had almost monolayer-dispersed Cr_2O_3 on
795 the ZrO_2 surface. The same catalyst composition also exhibited the best catalytic activity in
796 hydrocracking of IPB, DIPB, and TIPB at 250°C, and this can be attributed to the presence of
797 highest concentration of protonic acid sites in this catalyst. The formation of protonic acid sites is,
798 in turn, linked to the interaction between the chromium-oxygen double bond at 1035 cm^{-1} and H_2.
799 The presence of strong Lewis acid sites also contributed in stabilizing the electrons throughout the
800 creation of protonic acid sites. The percentage yield of products, C_3-C_8, for the catalysts used in
801 hydrocracking IPB, DIPB, and TIPB are shown in Figure 14.

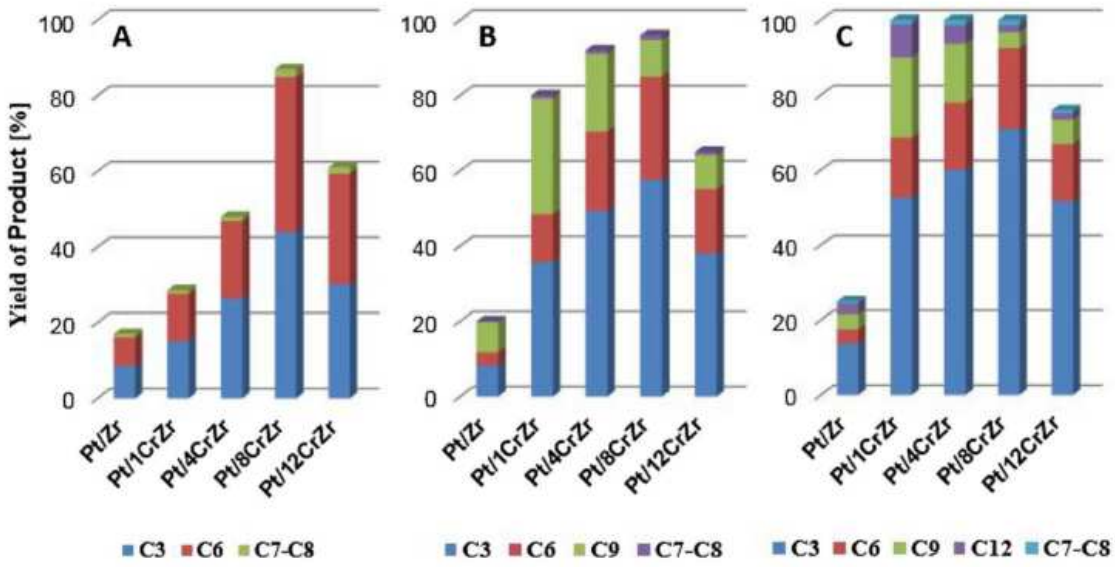

802

Figure 14. Percentage yield of products in hydrocracking A) isopropylbenzene (IPB), B) 1,4-diisopropylbenzene (DIPB) and C) 1,3,5-triisopropylbenzene (TIPB) for Pt/CrZr. Reproduced with permission from [126]

The porosity of catalysts in cracking reactions is, in general, of great significance in determining the effectiveness and preference of one catalyst over the other. For example, the catalytic cracking of 1,3,5-triisopropylbenzene using a mesoporous aluminosilicate (HMAS-5) catalyst resulted in much higher conversion, and higher selectivity towards benzene and isopropylbenzene, as compared to that when HZSM-5 was used [127]. This was attributed to the difference in porosity of the two catalysts, where the 1,3,5-triisopropylbenzene molecules were relatively large compared to the narrow channels of HZSM-5, lowering the accessibility to these sites, while the mesoporosity of HMAS-5 was more suitable for this type of reactants. The same cracking reaction was performed for HMAS-5 and HA1-MCM-41 catalysts [127]. It was found that the former catalyst showed better conversion, and this was because of its higher acidity with reference to the latter catalyst.

The production of BTX-rich light aromatics from light cycle oil (LCO) via hydrocracking was tested for a series of catalysts in [128]. Sulfided metals, NiMo-S, CoMo-S, and Mo-S were supported on a hybrid zeolite mixture of H-Beta and H-ZSM-5 with different compositions. Among the three catalyst analysed, Mo-S/H-Beta (90 wt%)-H-ZSM5 (10 wt%) yielded the most quantity of BTX in the hydrocracking of tetralin. This favoured combination was attributed to the moderate power of Mo-S in hydrogenation and the role H-ZSM-5 exhibited in promoting the dealkylation of alkyl-aromatics into BTX. Therefore, this catalyst presented highly selective hydrocracking behaviour, particularly at 6 MPa, since its metallic and acidic functions were properly balanced to achieve high BTX selectivity. More studies related to LCO upgrading into BTX can be found in the review article [129]. When naphtha is used as reformer feed in hydrocracking it is first hydro-treated for olefins removal by saturation, and as well, hydro-desulfurized and hydro-denitrogenated to remove sulfur and nitrogen compounds. This is important because olefinic compounds are undesirable in reformer feeds since they act as precursors for coke, while sulfur and nitrogen cause catalyst poisoning. During catalytic reforming, the reducing atmosphere promotes the formation of hydrogen sulphide and ammonia, which can

compromise the catalyst performance. A patent is granted for an integrated hydrocracking process for the production of ultra-low sulfur products of high octane gasoline and high aromatic naphtha from high aromatic middle distillate streams [130]. The feed is initially subjected to hydro-treatment, at a predetermined pressure, for the removal of heteroatoms such as sulfur and nitrogen. A different integrated hydrocracking process is patented for the production of olefinic and aromatic petrochemicals, in which the coker liquid produced after cracking is recycled in order to recover the petroleum coke [131].

In addition, three patents related to novel catalyst composition are published for middle distillate hydrocracking. The first is composed of 0.5-10 wt% zeolite β having an acidity of 20 to 400 nmol/g (a measure of Brønsted acid sites density in a catalyst), and an average domain size from 800 to 1500 nm^2, 0-5 wt% zeolite USY having an acid site distribution index (ASDI) between 0.05 and 0.12, with higher zeolite β concentration than zeolite USY, a catalyst support and metal [132]. The second patented catalyst is composed of zeolite β having an acidity of 20 to 50 μmol/g and an average crystal size between 300 to 800 nm, in addition to zeolite USY (with lower zeolite β concentration than zeolite USY), a support containing an amorphous silica aluminate and a second support material, and at least one metal [133]. While the third catalyst consists of 40 wt% to 70 wt% of a zeolite USY (ASDI between 0.05-0.18), amorphous silica alumina carrier, a second alumina, and 0.1 to 10 wt % noble metal, forming a catalyst BET surface area between 450 to 650 m^2/g [134].

Finally, we provide in Table 1, a summary of common catalysts and reaction conditions and products in hydrocracking different aromatic feeds, and Decalin (a bicyclic organic compound).

Table 1. Common catalysts used for hydrocracking various aromatic compounds

Feed	**Main product (Yield, wt.%)**	**Catalyst**	**Temperature (ºC)**	**Pressure (MPa)**	**LHSV (L)/WHSV (W) (h^{-1})**	**Reference**
Tetralin	BTX (54.3)	NiMo-S/H-Beta(90)-HZSM-5(10)	425	4	2 (W)	[135]

	(40.7) (48.1)	Ni/H-Beta zeolite	450	4	2 (W)	[7]
		Ni-Sn/H-Beta zeolite	450	4	2 (W)	[136]
	(54.2) Aromatics (20.1 mol%)	CoMo/Beta zeolite	370	8	1.6 (L)	[11]
		NiMo-S/ Al_2O_3-Y	310	4	NA	[137]
	Decalin isomers, light naphthenes (40.8, 21.2)	NiW/USY zeolite	340	4	2 (L)	[138]
	Naphthenes (44.1)	NiW/Al_2O_3-USY and NiW/P-USY + Al_2O_3 (phosphorus modified)	350	4	2 (L)	[139]
Decalin	C_9^- hydrocarbons (40)	Ir/H,A-Beta zeolite (A: alkali metal cation)	272	5.2	0.4-0.5 (L)	[140]
	Isomerization products (33.8)	MoS_2/MA (mesoporous alumino-silicates)	400	5	NA	[141]
Light cycle oil	High octane gasoline, ultra-low sulfur diesel (43.4, 52.5)	FC-24	400	8	1 (L)	[142], [143]
	High octane gasoline (NA)	NiMo/Al_2O_3-HY zeolite	400	7	1.3 (L)	[144]
	C_5^+ liquid yield (97.8)	NiMo/Al_2O_3-HY zeolite	400	8	0.8 (L)	[145]
	BTX (29.2)	Mo-S/ H-Beta (90 wt%)-H-ZSM5 (10 wt%) zeolite	425	6	2(W)	[128]

	Gasoil (80)	Pt/Y zeolite, Ir/Y zeolite	290-350	7	1-3 (W)	[146]
1-methylnaphthalene	BTX (42.3)	Ni_2P/Beta zeolite	380	6	0.5 (L)	[124]
	(alkyl)benzene (80)	NiMoS/alumina-mixed USY zeolites	360	5	NA	[8]
Naphthalene	BTX (94.4)	Ni_2P/Beta zeolite	400	3	3 (L)	[125]
	Benzene, toluene, ethylbenzene (33, 18, 13)	$FeSO_4$-H_2O (20 wt.%) Fe_2O_3 (20 wt.%), Al_2O_3 (20 wt.%) and sulfur (40 wt.%) mixture	425	10	NA	[147]
Pyrolysis fuel oil	BTX (31.3, 52)	CoMo/Beta zeolite	370	8	1.6 (L), 0.2 (L)	[11], [148]
Isopropylbenzene	C_3, C_6 (43, 40)	Pt/Cr_2O_3-ZrO_2	250	NA	NA	[126]
Bio-oil	Olefins, iso-paraffins (26.1, 23.7)	Ni/SiO_2–Al_2O_3 + CuO	425	9.7	NA	[30]

* NA: information not available in the cited reference

3.2 Upgrading of heavy petrochemical feedstock

In this section, we present recent work concerned with catalyst design for hydrocracking of heavy petrochemical feeds.

The performance of vacuum gas oil hydrocracking was evaluated for the use of β zeolite with and without carbon nanotubes (CNTs) as the catalyst, along with Ni and Mo impregnated on the zeolite/alumina support [149]. The results of the study showed that by incorporating CNTs into the catalyst support, its mesoporosity and volume increased significantly, however, the total Brønsted acid sites decreased. Also, among the zeolites tested, the one in which carbon nanotubes were added exhibited highest hydrocracking activity due to the creation of mesopores that ease the accessibility to acid sites. Furthermore, when zeolite to alumina ratio was increased, the cracking

activity was improved and became even more pronounced for the catalyst synthesized using carbon nanotubes. Yet, for similar conversion levels, the selectivity to middle distillate and naphtha was considerably reduced for the CNT-based zeolite because of the simultaneous decrease in the Brønsted acid sites. Therefore, it is important to enhance the mesoporosity of zeolites without reducing the strength of their acid sites, in order to improve the catalytic conversion of vacuum gas in hydrocracking processes.

Other authors [150] used composite catalysts composed of different types of zeolites for hydrocracking of vacuum gas oil. In the latter study, Y-β zeolite-zeolite composites were synthesized with various β to Y zeolites ratios. The prepared composite was seen to have hierarchical pores system because of the Si and/or Al being extracted from the Y-zeolite, and the intercrystalline spaces due to the polycrystallinity of nano-β zeolites in the shell. After running the hydrocracking reaction for vacuum gas oil using the composite zeolites of a core-shell structure as catalysts, it was observed that the Si/Al ratio in the zeolite had a significant impact on the performance of the cracking process. Zeolites with comparatively high Si/Al ratio facilitated the hydrocracking by showing higher activity and enhanced selectivity of middle distillates oil. Also, these zeolites increased the yield of jet fuel and the aromatic content of naphtha, as compared to catalysts with lower Si/Al ratio because of the decrease in acid density and increase in external surfaces of the catalyst. Selectivity towards heavy naphtha, jet fuel and middle distillate over the composite catalysts were 14.34 wt%, 43.11 wt% and 73.47 wt% for higher Si/Al ratio, compared to 13.66 wt%, 41.97 wt% and 72.62 wt% for lower Si/Al ratio, respectively.

An invention related to a combined hydrodesulphurization (HDS) and hydrocracking process for a heavy hydrocarbon feed is presented in a patent [151], in which these processes are simultaneously carried out at a temperature of 350-475°C and a pressure of 2500-4500 kPa. The catalyst used in the proposed invention is composed of a solid acid catalyst and HDS catalyst. The solid acid catalyst is an alumino-silicate zeolite having a SiO_2/Al_2O_3 molar ratio of 50-120, whereas the HDS catalyst comprises of 1-30 wt% of one or more elements from Group 6 of the periodic table, and 0.1-10 wt% of one or more elements from groups 9 and 10 of the periodic table. Under the aforementioned conditions, the inventors claim an efficient HDS and hydrocracking of a heavy hydrocarbon that is rich in sulfur and aromatic compounds with a significantly improved selectivity to mono-aromatic hydrocarbons. Furthermore, the performance of Na-Y and H-Y

molecular sieves as hydrocracking catalysts for heavy oil has also been presented in the literature [152]. The patented work for Na-Y provides an average grain diameter between 2-5 μm, and total pore volume mostly accounting for pores having diameters in the range of 1-10 nm [152]. H-Y molecular sieve, used as acidic component of the catalyst, provided improved cracking activity and product selectivity due to its relatively large crystal grains.

An innovative patented method for two-stage hydrocracking of challenging feeds to produce jet and diesel boiling range products is proposed by Dandekar et al. [153]. The challenging feedstock includes high aromatics content, low American Petroleum Institute (API) gravity, and low cetane number, and is hydrocracked to form distillate fuel products in a system having a minimum of two stages. While the first stage carries out preliminary hydro-treatment and/or hydrocracking, the second stage involves further hydrocracking in the presence of USY catalyst with supporting noble metal allowing an increased yield production of the distillate fuel.

In most catalytic reactions, nano-catalysts have shown great advantages over bulk catalysts. For example in cracking of tar, an undesirable by-product in biomass conversion, Ni-Co/Si-P nano-catalysts succeeded in cracking 99% of the tar, which is a considerable improvement compared to 91% cracking from bulk catalyst of the same composition at catalytic bed temperature of 800ºC [154]. This improvement was attributed to several important features of the catalyst, such as particle size, surface area and porosity. For example, their mesoporosity and large surface area allowed the active Ni sites to be better dispersed and thus, became more accessible to larger tar molecules, enhancing the selectivity towards smaller molecules such as H_2, CH_4, CO and CO_2.

A novel hydrocracking nano-catalyst consisting of nickel oxide nanoparticles supported on alumina nanoparticles, with particle size range between 30-100 nm, is patented in [155]. The alumina to nickel oxide nanoparticles weight ratio is in the range of 99-500, and the alumina nanoparticles are present in an amount of 99 wt% of catalyst.

As a summary, we present in Table 2 a list of common catalysts and reaction products in hydrocracking heavy petrochemicals. Detailed discussion on the use of MoS_2 as the main catalyst for heavy oil upgrading is presented in the review article recently published [156].

925 **Table 2.** Common catalysts used for hydrocracking heavy petrochemicals

Feed	Main product (Yield, wt.%)	Catalyst	Temperature (°C)	Pressure (MPa)	LHSV (L)/WHSV (W) (h^{-1})	Reference
Vacuum gas oil	Middle distillates and naphtha (15-60, 12-26)	NiMoP/USY (acid leached zeolite)	345	10.3	1 (W)	[157], [158]
		NiMo/CNT-modified Beta zeolite	350	10.3	1-2 (W)	[149]
		NiMo/Y zeolite cores and Beta-zeolite shells	NA	15.7	1 (W)	[150]
		NiMo/Y zeolite-Al_2O_3	410	16	0.71 (L)	[159]
		NiMo/zeolite-Al_2O_3 (zeolite: Y, recrystallized Y, Beta)	410	16	0.71 (L)	[160]
		Zr/Y zeolite	360	8	2 (L)	[161]
Vacuum gas oil with wax	Liquid yield (95-98)	NiMo/SiO_2-Al_2O_3	330-410	9.5	1.3 (L)	[162]
Vacuum residue	Vacuum gas oil, middle distillates (34.5, 25.7)	$LMo(CO)_3$ (L: 5-phenyl-1-pentyne)	430	8	NA	[163]
	Vacuum gas oil (35.5)	Mo precursor-triphenylphosphine (TPP) ligands	410	11	NA	[164]
Gudao vacuum residue	Gasoline and diesel (56.6)	CoMo/CNT	430	8	NA	[165]
Coal tar	Liquid yield (94.8)	Mo/modified bauxite	430	12.5	NA	[166]
	Liquid yield (91.9)	Ni-W/Al_2O_3	418	7.3	NA	[167]

Tar	Gaseous yield (H_2 24 vol %, CO 16 vol %)	Ni-Co/Si-P nanoparticles	800	NA	NA	[154]

* NA: information not available in the cited reference

3.3 Hydrocracking of paraffinic hydrocarbons

Nanomaterials and nano-sized zeolites have become increasingly popular in the development of catalysts for hydrocracking of paraffinic compounds, due to their superior performance as compared to their conventional counterparts. Graphene nanoplatelets (GNPs), for instance, were combined with reduced NiO and zeolite-Y to obtain a GNP/NiO-ZY composite catalyst for heptane hydrocracking in [168]. The study revealed that with the incorporation of GNPs into the catalyst, the conversion was improved by 31% at 350^{o}C and by 6% at 400^{o}C as compared to reduced NiO-ZY without GNPs. The former catalyst also exhibited superior stability after 20 h of time-on-stream, and favored the cracking into lighter molecules as shown by the selectivity measurements. The highest selectivity was reported towards propane for reduced GNP/NiO-ZY, whereas reduced NiO-ZY favored a high selectivity towards iso-butane and n-hexane. Furthermore, the use of reduced GNP/NiO-ZY resulted in higher selectivity towards ethylene and lower selectivity towards ethane as compared to reduced NiO-ZY, suggesting that the hydrogenation of ethylene to ethane over the metal nanoparticles was not as effective for GNP/Ni-ZY. The utilization of nano-zeolites was demonstrated, for example, in [169] and [170], where heptane was hydrocracked at 350^{o}C and 400^{o}C using NiO-WO_3 particles supported by nano-sized zeolite Y in both particle form [169] and fiber form [170]. The nano-sized zeolite [169] was obtained by ball milling commercial zeolites, having silica to alumina ratio of 30, at optimized conditions of 1000 rpm ball milling speed for short durations [171]. The nano-sized particles exhibited superior performance with respect to the overall conversion rate as compared to micro-sized zeolites. This is attributed to the higher surface area, and thus, increased active sites of the nanoparticles.

Both the structure and composition of the catalyst play a vital role in modifying the performance of hydrocracking reactions. An example for this is presented in [172], where the inactive composite TiO_2/Al_2O_3 aerogel made from Al_2O_3 nanofilaments was treated by hydrogen at high temperatures

of 650-850ºC. As a result of the hydrogen treatment, the composite was activated and was later used as an efficient catalyst for cracking of propane into alkenes. The boost in activation occurred due to the self-organization of the composite nanofilaments into the η-Al_2O_3 nanocrystalline hollow nanotubes. The number of nanotubes then increased and they became more oriented, and bundles of these packed nanotubes were created. The TiO_2/Al_2O_3 composite had mesoporous structure, and when used for the cracking of propane, yielded propylene as the main product, with catalytic activity of 0.1 mmol/g×s at 650ºC, and 68% selectivity. At higher temperatures, specifically at 750ºC, the yield of propylene increased to 0.4 mmol/g×s but for a lower selectivity of 50%. Therefore, the changes in structure of the composite catalyst following the hydrogen treatment not only activated them as catalysts for propane conversion, but also increased their efficiency compared to commercial platinum/alumina supported catalyst.

Additionally, Pt/ZSM-22 catalyst was used for cracking n-decane, n-nonadecane and pristane, in which its micropores resulted in creating mainly linear and cracked fragments [173]. The results showed that the hierarchical ZSM-22 contributed to reorganizing the distribution of Brønsted acidity, and thus achieving superior performance. For instance, in the hydrocracking of n-decane, the selectivities towards the cracked products were substantially different among the conventional and hierarchical ZSM-22. The composition of the C_5 cracked product fraction in conventional ZSM-22 was composed of 60% n-pentane, and 40% isopentane till 90% hydrocracking, whereas in the hierarchical ZSM-22, isopentane represented 55% and n-pentane 45% of the C_5 fraction. The higher isopentane content in the cracked products from the hierarchical catalyst was attributed to the higher content of dibranched isomers in the isodecanes.

Bi-functional Pt-loaded MFI zeolite nanosheets were synthesized and used as catalysts for the hydrocracking of n-decane [174]. The results showed that the production of C_5 from the cracking was inhibited because of the restricted shape-selectivity feature of the MFI type pores. This observation was made for the MFI nanosheets, as well as for the bulk crystals ZSM-5 zeolite. In addition, the formation of 2-methylnonane was reduced by the nanosheets as compared to the bulk ZSM-5. This was caused by short diffusion path due to the short channels of the nanosheets, leading to low diffusion of the 2-methylnonane product.

In Table 3, we present a list of recently developed catalysts for hydrocracking of paraffinic hydrocarbons, and the reaction conditions and products that were obtained in the referenced studies.

Table 3. Common catalysts used for hydrocracking various paraffinic hydrocarbons

Feed	**Main product (Yield, wt.%)**	**Catalyst**	**Temperature (ºC)**	**Pressure (MPa)**	**LHSV (L)/WHSV (W)(h^{-1})**	**Reference**
n-paraffin	Linear paraffins, mono-branched compounds (NA)	Pt/SiO_2-Al_2O_3	270-330	2-8	0.33-1 (W)	[175]
Heptane	Propane (NA)	GNP (graphene nanoplatelets)/ NiO-Y zeolite	350-400	0.5	4.2 (L)	[168]
	n-hexane, iso-hexane (NA)	NiO-WO_3 /Y zeolite	350-400	0.5	4 (W)	[169]
n-Heptane, n-Hexane	C_1-C_5 products (66.7)	Activated WO_3/TiO_2	250-350	0.5-2.5	0.8-2 (L)	[176]
Hexadecane	C_5-C_{15} products (51.9)	NiMo/USY-Al_2O_3	340	4	4 (W)	[177]
	C_9-C_{15} products (86)	Pt-H-Beta-25	240	4.5	NA	[178]
n-Hexadecane	C_4-C_7 (51.6)	Pt-H-ZSM-5 (Hierarchical)	280	9.65	NA	[179]
Propane	Propylene (35)	TiO_2/Al_2O_3	800	NA	NA	[172]
Squalane	Middle distillates (NA)	NiMo/[γ-Al_2O_3 + (Ni)/USY]	346-352	6	1 (L)	[180]

n-decane	C_4-C_7 products (NA)	Pt-loaded MFI zeolite nanosheets	140-230	NA	NA	[174]
	C_6 hydrocarbons (NA)	Ni–Mo/$Cs_{1.5}H_{1.5}PW/Al_2O_3$	300	3	NA	[181]

* NA: information not available in the cited reference

3.4 Hydrocracking of vegetable oils

The cracking of palm oil into jet biofuel with high alkane and low arene yield was performed using various Ni/zeolite catalysts [182]. Among the five tested zeolites, Ni/SAPO-34, Ni/MCM-41, Ni/HY, Ni/SAPO-11 and Ni/H-β, the presence of SaPO-34 zeolite with Ni loading lead to the best upgrading process. The Ni/SAPO-34 catalyst showed the maximum alkane selectivity of 65%, and concurrently, the minimum arene selectivity of 11%. Furthermore, as the Si/Al weight ratio in the zeolite decreased from 11 to 5, the resulting yield of alkanes in the biofuel increased, from 71% to 80% with a reduction in the arene yield from 29% to 20%. Varying the amount of Ni in the Ni/HY catalyst had negligible impact on the content of alkane and arene in the final product.

Castor oil was hydro-processed in an attempt to produce a high yield of aviation fuel using Ni supported on different acidic zeolites, i.e. zeolites of different forms and/or with various Si/Al ratio [183]. It was shown that various fuel range alkanes, C_8-C_{15}, can be obtained when adjusting the degree of hydro-deoxygenation and hydrocracking. The catalysts with moderate acidity employed in the study were able to promote the conversion of castor oil into high yields of bio-aviation fuel (91.6 wt%) with high isomerization selectivity. For example, hydrocracking over 25% Ni/USY–APTES– MCM-41 (APTES, (3-Aminopropyl)-tri-ethoxysilane: 7.5%) catalyst at 300^{o}C yielded 80.3 wt% of C_8-C_{15} hydrocarbons.

Additionally, non-sulfided NiMoCe/Al_2O_3 catalyst was developed to catalyse the hydrocracking of Jatropha oil in an attempt to produce green diesel [184]. The produced oil mainly consisted of C_{15} to C_{18} straight chain alkanes having optimum catalytic performance at 370^{o}C and 3.5 MPa. At these conditions the yield and selectivity of C_{15} to C_{18} were 80% and 90%, respectively, with a conversion of 89%. The results show that by doping a predetermined amount of Ce onto the NiMo/

Al_2O_3 catalyst, improvements in the conversion and selectivity levels are visible, and a stable catalytic performance is noticed.

Long chain hydrocarbons derived from safflower oil were hydrocracked by Ni–Mo, Ni–W carbides, Pt and triflic acid based catalysts supported on mesoporous SBA-15 [185]. The yield of naphtha, C_5 to C_9, was between 15 to 30 wt%, while that for light products was less than 5 wt%. Out of the catalysts prepared in this study, two acid-based catalysts exhibited outstanding performance producing naphtha and light products with yields higher than 30% and 15%, respectively, owing to the significant influence of surface acidic active sites on the cracking reactions of long chain hydrocarbons.

Additionally, the use of composite catalysts for hydrocracking soybean oils was shown to improve the overall performance of the process as compared to using single catalysts [186]. Particularly, NiMo-supported zeolite–alumina catalysts were effective for the reaction, and the product selectivity was highly dependent on the kind of zeolite used. For instance, NiMo/USY-Al_2O_3 catalyst exhibited high selectivity for diesel fraction, while NiMo/Beta-Al_2O_3 catalyst showed higher selectivity for the gasoline fraction, and thus, it was demonstrated that gasoline and diesel fractions could be produced selectively by selecting the proper kind of zeolite in the zeolite–alumina composite supported NiMo catalysts.

A summary of the most common hybrid catalysts used for hydrocracking vegetable oil is shown in Table 4.

Table 4. Common catalysts used for hydrocracking vegetable oils

Feed	**Main Product (Yield, wt.%)**	**Catalyst**	**Temperature (°C)**	**Pressure (MPa)**	**LHSV (L)/WHSV (W) (h^{-1})**	**Reference**
Vegetable oil	n-C_{17}, n-C_{18} alkanes (NA)	sulfided NiMo/Al_2O_3	400	9.2	NA	[187]
	C_5–C_9 (15-30)	NiMo, NiW, and Pt/SBA-15	340	NA	NA	[185]

Castor oil	C_8-C_{15} (80.3)	25% Ni/USY–APTES–MCM-41 (APTES: 7.5%)	300	3	2 (W)	[183]
Palm oil	C_{15}–C_{17} (65)	10 wt.% Ni_2P/SiO_2	380, 400	4	2 (W)	[188]
Rapeseed oil	C_{17} and C_{18} n-alkanes (~20, ~70)	sulfided $NiMo/Al_2O_3$	260-340	7	1 (W)	[189]
Jatropha oil	C_{15}–C_{18} alkanes (80)	non-sulfided $NiMoCe/Al_2O_3$	370	3.5	0.9 (L)	[184]
Sunflower oil-gas oil	C_{15}–C_{18} alkanes (NA)	NiO(3%)–MoO_3(12%)–γ-Al_2O_3 with various amounts of β zeolite	330	6	2 (W)	[190]
Sunflower oil	High paraffin (73.7–73.9)	$CoMo/Al_2O_3$	380	4-6	1 (L)	[191]
Soybean oil	Gasoline (NA)	Zeolite (ZSM-5) supported PtNiMo sulfides	420	>1	6.13 (W)	[192]
Methyl palmitate	Jet fuel (NA)	HPW (phosphotungstic acid)-Ni/MCM-41	390	2	NA	[193]

* NA: information not available in the cited reference

4. Conclusions and perspectives

In this paper, we examined the current literature on synthesis, characterization and testing of hydrocracking catalysts for a wide range of applications. Our review showed that bi-functional catalysts, consisting of an acid support and impregnated metal particles, are the dominant class of

catalysts used in hydrocracking processes. Novel techniques for synthesizing such catalysts, especially zeolite supports, were identified in the literature and presented in detail. In addition, well-established performance criteria were used to evaluate and compare the performance of various hydrocracking catalysts, focusing on four major types of feeds: (a) aromatic compounds, (b) heavy petrochemicals, (c) paraffinic hydrocarbons and (d) vegetable oil. Based on the findings discussed in this review, it can be concluded that the efficiency of hydrocracking reactions relies on a number of intrinsic (catalyst-related) and extrinsic (process-related) factors:

i. Intrinsic factors:

It was shown that the catalysts' porosity, morphology, structure, shape selectivity and composition all had significant impact on the overall performance of hydrocracking different fuels. For most feed molecules considered herein, the use of nano-sized and/or mesoporous zeolites was associated with improved conversion and reaction rates as compared to conventional zeolites, due to their large surface area and high accessibility to acid sites. Moreover, incorporating CNTs in the zeolite synthesis was identified as a promising method to produce hierarchical zeolites having both micro- and mesoporosity leading to increased catalytic activity in hydrocracking reactions. However, with the addition of CNTs, the Brønsted acid sites in the catalyst decreased causing a reduction in the selectivity to middle distillate and naphtha, and thus, careful control over the amount of CNTs added is essential for a proper balance between acidity and induced mesoporosity. Moreover, variations of pore sizes of the zeolite allow different reaction routes to take place, since molecules' accessibility to the reaction sites may be facilitated or suppressed according to their relative size. The addition of binders to the catalyst also has various effects on the performance of hydrocracking as they change the overall catalyst's mechanical and thermal characteristics, acidity, coke deposition level, and porosity by inducing a mesoporosity to the catalyst. The positive impact of adding binders can sometimes match or exceed the effects of hierarchically structuring catalysts.

It was noticed that Ni-based catalysts (often supported by β zeolite) have been extensively used for hydrocracking aromatic compounds for the production of BTX. Bimetallic Ni-Mo catalysts supported by zeolite Y have been widely used for heavy vacuum gas oil hydrocracking, whereas alumina supported Ni-Mo catalysts were favoured for hydrocracking of vegetable oil. Furthermore, catalyst deactivation is a vital parameter for assessing the material performance during the reaction. Nano-sized β zeolite loaded with Ni_2P, Ni_2P/β-N, when compared to micro-

sized β zeolite with similar loading, Ni_2P/β-M, showed better stability and resistance to coke formation in the conversion of naphthalene into BTX, in addition to the improved catalytic activity. Also, increasing the Si/Al ratio of protonic zeolites increases their stability during the reaction and prevents easy de-alumination.

ii. Extrinsic factors:

The type of feed being hydrocracked significantly affects the reaction pathway and thus, each type of feed undergoes a distinct reaction mechanism. Apart from the feed nature, the process conditions play a crucial role in determining the performance of hydrocracking. Increasing the hydrocracking temperature typically results in faster cracking on acid sites, however, facilitates coking and catalyst deactivation. Additionally, very high temperatures limit the hydrocracking of aromatic compounds. Higher hydrogen partial pressure enhances the conversion of aromatics into saturated products, thus, the optimal conditions for hydrocracking aromatic hydrocarbons are high pressure, high hydrogen to feed ratio, and lowest possible temperature. Therefore, process conditions should carefully be selected according to the fuel type and products of interest.

Advancement in zeolite and nanomaterial synthesis opens the door for further progress in the development of new catalysts, or improvement of current catalysts. It is expected that the development of nano-sized and/or mesoporous zeolite supports will continue to be the focal point of future research in this field. However, if current challenges, such as lacking scalability of material synthesis processes and difficulty in achieving hierarchically porous systems, cannot be overcome, the need for more innovative new material systems will arise in the future. One possible future direction in the development of new hydrocracking catalysts is the development of hybrid supports consisting of zeolites and carbon-based nanomaterials (e.g. CNTs, CNS, Graphene, GO, etc.) which possess large specific surface area and high thermal stability. Although nano-carbons cannot be solely used as supports for hydrocracking catalysts due to the missing acid sites, they could serve as templates for the synthesis of hierarchical zeolites and, in addition, support additional metal particles which catalyse hydrogenation and de-hydrogenation reactions.

We hope that this review has given the reader an overview of recent advances in the development of hydrocracking catalysts and allowed identifying current needs and challenges involved in

upgrading of fossil and renewable fuels. We also hope that it will inspire the reader and spark new ideas in the design of new catalysts to further advance this active field of research.

Acknowledgements

The authors gratefully appreciate the financial support from the Abu Dhabi Department of Education and Knowledge through the ADEK Award for Research Excellence (AARE) 2017 [grant number AARE17-270]. This publication is partially based upon work supported by the Khalifa University of Science and Technology [grant number RC2-2018-024].

References

[1] R. Sahu, B. J. Song, J. S. Im, Y. P. Jeon, and C. W. Lee, "A review of recent advances in catalytic hydrocracking of heavy residues," *J. Ind. Eng. Chem.*, vol. 27, pp. 12–24, 2015.

[2] H. B. Park, K. D. Kim, and Y. K. Lee, "Promoting asphaltene conversion by tetralin for hydrocracking of petroleum pitch," *Fuel*, vol. 222, no. February, pp. 105–113, 2018.

[3] M. S. Rana, V. Sámano, J. Ancheyta, and J. A. I. Diaz, "A review of recent advances on process technologies for upgrading of heavy oils and residua," *Fuel*, vol. 86, no. 9, pp. 1216–1231, 2007.

[4] J. Mosio-Mosiewski and I. Morawski, "Study on single-stage hydrocracking of vacuum residue in the suspension of Ni-Mo catalyst," *Appl. Catal. A Gen.*, vol. 283, no. 1–2, pp. 147–155, 2005.

[5] J. Scherzer and fl. J. Gruia, *Hydrocracking Science and Technology*. New York: Marcel Dekker Inc., 1996.

[6] J. G. Speight, "Thermal Decomposition of Hydrocarbons," in *Handbook of Industrial Hydrocarbon Processes*, Elsevier Inc., 2011, pp. 395–428.

[7] Y. Choi, J. Lee, J. Shin, S. Lee, D. Kim, and J. K. Lee, "Selective hydroconversion of naphthalenes into light alkyl-aromatic hydrocarbons," *Appl. Catal. A Gen.*, vol. 492, pp. 140–150, 2015.

[8] J. Il Park, J. K. Lee, J. Miyawaki, Y. K. Kim, S. H. Yoon, and I. Mochida, "Hydro-conversion of 1-methyl naphthalene into (alkyl)benzenes over alumina-coated USY zeolite-supported NiMoS catalysts," *Fuel*, vol. 90, no. 1, pp. 182–189, 2011.

[9] A. Ishihara, T. Itoh, H. Nasu, T. Hashimoto, and T. Doi, "Hydrocracking of 1-methylnaphthalene / decahydronaphthalene mixture catalyzed by zeolite-alumina composite supported NiMo catalysts," *Fuel Process. Technol.*, vol. 116, pp. 222–227,

2013.

[10] V. Calemma, R. Giardino, and M. Ferrari, “Upgrading of LCO by partial hydrogenation of aromatics and ring opening of naphthenes over bi-functional catalysts,” *Fuel Process. Technol.*, vol. 91, no. 7, pp. 770–776, 2010.

[11] D. P. Upare *et al.*, “Cobalt promoted Mo/beta zeolite for selective hydrocracking of tetralin and pyrolysis fuel oil into monocyclic aromatic hydrocarbons,” *J. Ind. Eng. Chem.*, vol. 35, pp. 99–107, 2016.

[12] M. Romero *et al.*, “Preliminary experimental study on biofuel production by deoxygenation of Jatropha oil,” *Fuel Process. Technol.*, vol. 137, pp. 31–37, 2015.

[13] M. M. Gui, K. T. Lee, and S. Bhatia, “Feasibility of edible oil vs. non-edible oil vs. waste edible oil as biodiesel feedstock,” *Energy*, vol. 33, no. 11, pp. 1646–1653, 2008.

[14] Y. W. Mirzayanti, F. Kurniawansyah, and D. H. Prajitno, “Zn-Mo / HZSM-5 Catalyst for Gasoil Range Hydrocarbon Production by Catalytic Hydrocracking of Ceiba pentandra Oil,” *Bull. Chem. React. Eng. Catal.*, vol. 13, no. 1, pp. 136–143, 2018.

[15] D. H. Prajitno, A. Roesyadi, M. Al-Muttaqii, and L. Marlinda, “Hydrocracking of non-edible vegetable oils with Co-Ni/HZSM-5 catalyst to gasoil containing aromatics,” *Bull. Chem. React. Eng. Catal.*, vol. 12, no. 3, pp. 318–328, 2017.

[16] A. Adrados, I. de Marco, B. M. Caballero, A. López, M. F. Laresgoiti, and A. Torres, “Pyrolysis of plastic packaging waste: A comparison of plastic residuals from material recovery facilities with simulated plastic waste,” *Waste Manag.*, vol. 32, no. 5, pp. 826–832, 2012.

[17] F. de Miguel Mercader, M. J. Groeneveld, S. R. A. Kersten, R. H. Venderbosch, and J. A. Hogendoorn, “Pyrolysis oil upgrading by high pressure thermal treatment,” *Fuel*, vol. 89, no. 10, pp. 2829–2837, 2010.

[18] P. M. Mortensen, J. D. Grunwaldt, P. A. Jensen, K. G. Knudsen, and A. D. Jensen, “A review of catalytic upgrading of bio-oil to engine fuels,” *Appl. Catal. A Gen.*, vol. 407, no. 1–2, pp. 1–19, 2011.

[19] I. Elizalde and J. Ancheyta, “Application of a three-stage approach for modeling the complete period of catalyst deactivation during hydrotreating of heavy oil,” *Fuel*, vol. 138, pp. 45–51, 2014.

[20] E. G. Fuentes-Ordóñez, J. A. Salbidegoitia, M. P. González-Marcos, J. L. Ayastuy, M. A. Gutiérrez-Ortiz, and J. R. González-Velasco, “Pt/ITQ-6 zeolite as a bifunctional catalyst for hydrocracking of waste plastics containing polystyrene,” *J. Mater. Cycles Waste Manag.*, vol. 17, no. 3, pp. 465–475, 2015.

[21] B. Akash, “Thermochemical depolymerization of biomass,” *Procedia Comput. Sci.*, vol. 52, no. 1, pp. 827–834, 2015.

[22] J. Rencoret *et al.*, “Lignin Composition and Structure in Young versus Adult Eucalyptus

globulus Plants," *Plant Physiol.*, vol. 155, no. 2, pp. 667–682, 2011.

[23] C. Xu, R. A. D. Arancon, J. Labidi, and R. Luque, "Lignin depolymerisation strategies: towards valuable chemicals and fuels," *Chem. Soc. Rev.*, vol. 43, no. 22, pp. 7485–7500, 2014.

[24] R. Lou and S. bin Wu, "Products properties from fast pyrolysis of enzymatic/mild acidolysis lignin," *Appl. Energy*, vol. 88, no. 1, pp. 316–322, 2011.

[25] R. Shu *et al.*, "Investigation on the structural effect of lignin during the hydrogenolysis process," *Bioresour. Technol.*, vol. 200, pp. 14–22, 2016.

[26] J. Yang, L. Zhao, S. Liu, Y. Wang, and L. Dai, "High-quality bio-oil from one-pot catalytic hydrocracking of kraft lignin over supported noble metal catalysts in isopropanol system," *Bioresour. Technol.*, vol. 212, pp. 302–310, 2016.

[27] X. Zhang, T. Wang, L. Ma, Q. Zhang, X. Huang, and Y. Yu, "Production of cyclohexane from lignin degradation compounds over Ni/ZrO2-SiO2catalysts," *Appl. Energy*, vol. 112, pp. 533–538, 2013.

[28] M. Misson, R. Haron, M. F. A. Kamaroddin, and N. A. S. Amin, "Pretreatment of empty palm fruit bunch for production of chemicals via catalytic pyrolysis," *Bioresour. Technol.*, vol. 100, no. 11, pp. 2867–2873, 2009.

[29] J. Wang *et al.*, "Liquefaction of kraft lignin by hydrocracking with simultaneous use of a novel dual acid-base catalyst and a hydrogenation catalyst," *Bioresour. Technol.*, vol. 243, pp. 100–106, 2017.

[30] S. K. Tanneru and P. H. Steele, "Direct hydrocracking of oxidized bio-oil to hydrocarbons," *Fuel*, vol. 154, no. 4, pp. 268–274, 2015.

[31] G. Busca, "Acidity and basicity of zeolites: A fundamental approach," *Microporous Mesoporous Mater.*, vol. 254, no. June 2016, pp. 3–16, 2017.

[32] X. Wang, X. Zhang, and Q. Wang, "N-dodecane hydroisomerization over Pt/ZSM-22: Controllable microporous Brönsted acidity distribution and shape-selectivity," *Appl. Catal. A Gen.*, vol. 590, p. 117335, 2020.

[33] P. S. F. Mendes, J. M. Silva, M. F. Ribeiro, P. Duchene, A. Daudin, and C. Bouchy, "Quantification of Metal-Acid Balance in Hydroisomerization Catalysts: A Step Further Toward Catalyst Design," *AIChE J.*, vol. 63, no. 7, pp. 2864–2875, 2017.

[34] W. Wang, C. J. Liu, and W. Wu, "Bifunctional catalysts for the hydroisomerization of: n-alkanes: The effects of metal-acid balance and textural structure," *Catal. Sci. Technol.*, vol. 9, no. 16, pp. 4162–4187, 2019.

[35] P. S. F. Mendes, J. M. Silva, M. F. Ribeiro, A. Daudin, and C. Bouchy, "Synergies, cooperation and other effects: a review for hydroconversion catalysts," *Catal. Today*, no. August, pp. 1–11, 2019.

[36] C. Pagis, C. Bouchy, M. Dodin, R. Martinez Franco, D. Farrusseng, and A. Tuel, “Hollow y zeolite single crystals: Synthesis, characterization and activity in the hydroisomerization of n -hexadecane,” *Oil Gas Sci. Technol.*, vol. 74, 2019.

[37] M. Hartmann, A. G. Machoke, and W. Schwieger, “Catalytic test reactions for the evaluation of hierarchical zeolites,” *Chem. Soc. Rev.*, vol. 45, no. 12, pp. 3313–3330, 2016.

[38] A. Feliczak-Guzik, “Hierarchical zeolites: Synthesis and catalytic properties,” *Microporous Mesoporous Mater.*, vol. 259, pp. 33–45, 2018.

[39] J. Pérez-Ramírez, C. H. Christensen, K. Egeblad, C. H. Christensen, and J. C. Groen, “Hierarchical zeolites: Enhanced utilisation of microporous crystals in catalysis by advances in materials design,” *Chem. Soc. Rev.*, vol. 37, no. 11, pp. 2530–2542, 2008.

[40] P. Robinson and G. E. Dolbear, “Hydrotreating and Hydrocracking: Fundamentals,” in *Practical Advances in Petroleum Processing*, no. June, 2007, pp. 177–218.

[41] M. T. Klein and G. Hou, “Mechanistic Kinetic Modeling of Heavy Paraffin Hydrocracking,” in *Practical Advances in Petroleum Processing*, vol. 5, Springer, New York, NY, 2007, pp. 187–204.

[42] J. W. Thybaut *et al.*, “Alkylcarbenium ion concentrations in zeolite pores during octane hydrocracking on Pt/H-USY zeolite,” *Catal. Letters*, vol. 94, no. 1–2, pp. 81–88, 2004.

[43] H. Kumar, “Mechanistic Kinetic Modeling of the Hydrocracking of Complex Feedstocks,” Texas A&M University, 2006.

[44] H. Kumar and G. F. Froment, “Mechanistic kinetic modeling of the hydrocracking of complex feedstocks, such as vacuum gas oils,” *Ind. Eng. Chem. Res.*, vol. 46, no. 18, pp. 5881–5897, 2007.

[45] J. W. Thybaut, G. B. Marin, G. V. Baron, P. A. Jacobs, and J. A. Martens, “Alkene protonation enthalpy determination from fundamental kinetic modeling of alkane hydroconversion on Pt/H-(US)Y-zeolite,” *J. Catal.*, vol. 202, no. 2, pp. 324–339, 2001.

[46] G. F. Froment, “Single event kinetic modeling of complex catalytic processes,” *Catal. Rev. - Sci. Eng.*, vol. 47, no. 1, pp. 83–124, 2005.

[47] C. Martínez and A. Corma, “Inorganic molecular sieves: Preparation, modification and industrial application in catalytic processes,” *Coord. Chem. Rev.*, vol. 255, no. 13–14, pp. 1558–1580, 2011.

[48] P. S. F. Mendes, J. M. Silva, M. F. Ribeiro, C. Bouchy, and A. Daudin, “Quantification of the available acid sites in the hydrocracking of nitrogen-containing feedstocks over USY shaped NiMo-catalysts,” *J. Ind. Eng. Chem.*, vol. 71, pp. 167–176, 2019.

[49] I. Petrov and T. Michalev, “Synthesis of Zeolite A: A Review,” in *Chemical Technologies*, 2012, no. 51, Book 9.1, pp. 30–35.

[50] M. Bulut and P. A. Jacobs, “Concepts for Preparation of Zeolite-Based Catalysts,” in *Synthesis of Solid Catalysts*, 2009, pp. 243–276.

[51] E. Koohsaryan and M. Anbia, “Nanosized and hierarchical zeolites: A short review,” *Chinese J. Catal.*, vol. 37, no. 4, pp. 447–467, 2016.

[52] Y. Qiu, L. Wang, X. Zhang, and G. Liu, “Different roles of CNTs in hierarchical HZSM-5 synthesis with hydrothermal and steam-assisted crystallization,” *RSC Adv.*, vol. 5, no. 95, pp. 78238–78246, 2015.

[53] Y. Wei, T. E. Parmentier, K. P. De Jong, and J. Zečević, “Tailoring and visualizing the pore architecture of hierarchical zeolites,” *Chem. Soc. Rev.*, vol. 44, no. 20, pp. 7234–7261, 2015.

[54] A. Parulkar, R. Joshi, N. Deshpande, and N. A. Brunelli, “Synthesis and Catalytic Testing of Lewis Acidic Nano-MFI Zeolites for the Epoxide Ring Opening Reaction with Alcohol,” *Appl. Catal. A, Gen.*, vol. 566, no. June, pp. 25–32, 2018.

[55] J. Zhao, Y. Yin, Y. Li, W. Chen, and B. Liu, “Synthesis and characterization of mesoporous zeolite Y by using block copolymers as templates,” *Chem. Eng. J.*, vol. 284, pp. 405–411, 2016.

[56] M. Choi, K. Na, J. Kim, Y. Sakamoto, O. Terasaki, and R. Ryoo, “Stable single-unit-cell nanosheets of zeolite MFI as active and long-lived catalysts,” *Nature*, vol. 461, no. September, 2009.

[57] P. Y. Looi, A. R. Mohamed, and C. T. Tye, “Hydrocracking of residual oil using molybdenum supported over mesoporous alumina as a catalyst,” *Chem. Eng. J.*, vol. 181–182, pp. 717–724, 2012.

[58] A. A. Dabbawala *et al.*, “Synthesis of nanoporous zeolite-Y and zeolite-Y/GO nanocomposite using polyelectrolyte functionalized graphene oxide,” *Surf. Coatings Technol.*, vol. 350, no. June, pp. 369–375, 2018.

[59] J. García-Martínez, K. Li, and G. Krishnaiah, “A mesostructured y zeolite as a superior FCC catalyst - From lab to refinery,” *Chem. Commun.*, vol. 48, no. 97, pp. 11841–11843, 2012.

[60] M. Khaleel, W. Xu, D. A. Lesch, and M. Tsapatsis, “Combining Pre- and Post-Nucleation Trajectories for the Synthesis of High FAU-Content Faujasite Nanocrystals from Organic-Free Sols,” *Chem. Mater.*, vol. 28, no. 12, pp. 4204–4213, 2016.

[61] M. Khaleel, A. J. Wagner, K. A. Mkhoyan, and M. Tsapatsis, “On the rotational intergrowth of hierarchical FAU/EMT zeolites,” *Angew. Chemie - Int. Ed.*, vol. 53, no. 36, pp. 9456–9461, 2014.

[62] S. W. Han, J. Kim, and R. Ryoo, “Dry-gel synthesis of mesoporous MFI zeolite nanosponges using a structure-directing surfactant,” *Microporous Mesoporous Mater.*, vol. 240, pp. 123–129, 2017.

[63] C. Li, Y. Ren, J. Gou, B. Liu, and H. Xi, “Facile synthesis of mesostructured ZSM-5 zeolite with enhanced mass transport and catalytic performances,” *Appl. Surf. Sci.*, vol. 392, pp. 785–794, 2017.

[64] L. Emdadi *et al.*, “Synthesis of hierarchical lamellar MFI zeolites with sequential intergrowth influenced by synthetic gel composition,” *Microporous Mesoporous Mater.*, vol. 275, no. July 2018, pp. 31–41, 2019.

[65] J. K. Reddy, K. Motokura, T. R. Koyama, A. Miyaji, and T. Baba, “Effect of morphology and particle size of ZSM-5 on catalytic performance for ethylene conversion and heptane cracking,” *J. Catal.*, vol. 289, pp. 53–61, 2012.

[66] Z. Huo *et al.*, “Synthesis of zeolite NaP with controllable morphologies,” *Microporous Mesoporous Mater.*, vol. 158, pp. 137–140, 2012.

[67] H. S. Shin, M. Opanasenko, C. P. Cabello, R. Ryoo, and J. Čejka, “Surfactant-directed mesoporous zeolites with enhanced catalytic activity in tetrahydropyranylation of alcohols: Effect of framework type and morphology,” *Appl. Catal. A Gen.*, vol. 537, pp. 24–32, 2017.

[68] S. Cheng, B. Mazonde, G. Zhang, M. Javed, and P. Dai, “Co-based MOR / ZSM-5 composite zeolites over a solvent-free synthesis strategy for improving gasoline selectivity,” *Fuel*, vol. 223, no. February, pp. 354–359, 2018.

[69] L. Domokos and C. Ouwehand, “Hydrocracking Catalyst,” US 2016/0074846A1, 2016.

[70] P. Shariaty and Z. Hashisho, “Carbon nanotube growth on zeolite Y to tailor its electric resistivity for resistive heating regeneration,” *Microporous Mesoporous Mater.*, vol. 277, no. November 2018, pp. 171–178, 2019.

[71] M. Babaei, M. Anbia, and M. Kazemipour, “Synthesis of zeolite/carbon nanotube composite for gas separation,” *Can. J. Chem.*, vol. 95, no. 2, pp. 162–168, 2016.

[72] N. Kosinov, C. Liu, E. J. M. Hensen, and E. A. Pidko, “Engineering of Transition Metal Catalysts Confined in Zeolites,” *Chem. Mater.*, vol. 30, no. 10, pp. 3177–3198, 2018.

[73] J. Kim, W. Kim, Y. Seo, J. C. Kim, and R. Ryoo, “N-Heptane hydroisomerization over Pt/MFI zeolite nanosheets: Effects of zeolite crystal thickness and platinum location,” *J. Catal.*, vol. 301, pp. 187–197, 2013.

[74] K. Polychronopoulou and A. M. Efstathiou, “Spillover of labile OH, H, and O species in the H2 production by steam reforming of phenol over supported-Rh catalysts,” *Catal. Today*, vol. 116, no. 3, pp. 341–347, 2006.

[75] N. D. Charisiou *et al.*, “Hydrogen production via the glycerol steam reforming reaction over nickel supported on alumina and lanthana-alumina catalysts,” *Int. J. Hydrogen Energy*, vol. 42, no. 18, pp. 13039–13060, 2017.

[76] K. Polychronopoulou, K. Giannakopoulos, and A. M. Efstathiou, “Tailoring MgO-based supported Rh catalysts for purification of gas streams from phenol,” *Appl. Catal. B*

Environ., vol. 111–112, pp. 360–375, 2012.

[77] K. C. Petallidou, K. Polychronopoulou, J. L. G. Fierro, and A. M. Efstathiou, "Low-temperature water-gas shift on Pt/Ce0.8La0.2O2-δ-CNT: The effect of Ce0.8La0.2O2-δ/CNT ratio," *Appl. Catal. A Gen.*, vol. 504, pp. 585–598, 2015.

[78] R. Wade, J. Vislocky, T. Maesen, and D. Torchia, "Hydrocracking catalyst and processing developments," *Pet. Technol. Q.*, vol. 14, no. 4, pp. 81–86, 2009.

[79] M. A. Ali, T. Tatsumi, and T. Masuda, "Development of heavy oil hydrocracking catalysts using amorphous silica-alumina and zeolites as catalyst supports," *Appl. Catal. A Gen.*, vol. 233, no. 1–2, pp. 77–90, 2002.

[80] E. Marceau, X. Carrier, and M. Che, "Impregnation and Drying," in *Synthesis of Solid Catalysts*, K. P. De Jong, Ed. 2009, pp. 59–82.

[81] K. S. Smith, "Metal Sorption on Mineral Surfaces: an Overview with Examples Relating to Mineral Deposits," *Soc. Econ. Geol.*, vol. 6, 1999.

[82] J. F. Lambert and M. Che, "The molecular approach to supported catalysts synthesis: State of the art and future challenges," *J. Mol. Catal. A Chem.*, vol. 162, no. 1–2, pp. 5–18, 2000.

[83] X. Liu *et al.*, "Zeta potential of beta zeolites: Influence of structure, acidity, pH, temperature and concentration," *Molecules*, vol. 23, no. 4, pp. 1–14, 2018.

[84] R. R. Barton, M. Carrier, C. Segura, J. L. G. Fierro, N. Escalona, and S. W. Peretti, "Ni/HZSM-5 catalyst preparation by deposition-precipitation. Part 1. Effect of nickel loading and preparation conditions on catalyst properties," *Appl. Catal. A, Gen.*, vol. 540, no. March, pp. 7–20, 2017.

[85] R. R. Barton *et al.*, "Ni/HZSM-5 catalyst preparation by deposition-precipitation . Part 2 . Catalytic hydrodeoxygenation reactions of lignin model compounds in organic and aqueous systems," *Appl. Catal. A, Gen.*, vol. 562, no. February, pp. 294–309, 2018.

[86] K. P. de Jong, "Deposition Precipitation," in *Synthesis of Solid Catalysts*, K. P. De Jong, Ed. 2009, pp. 111–134.

[87] G. Mul and A. S. Hirschon, "Effect of preparation procedures on the activity of supported palladium/lanthanum methanol decomposition catalysts," *Catal. Today*, vol. 65, no. 1, pp. 69–75, 2001.

[88] Y. M. Galeano, F. Negri, M. S. Moreno, J. Múnera, L. Cornaglia, and A. M. Tarditi, "Pt encapsulated into NaA zeolite as catalyst for the WGS reaction," *Appl. Catal. A, Gen.*, vol. 572, no. September 2018, pp. 176–184, 2019.

[89] S. Li, A. Tuel, F. Meunier, M. Aouine, and D. Farrusseng, "Platinum nanoparticles entrapped in zeolite nanoshells as active and sintering-resistant arene hydrogenation catalysts," *J. Catal.*, vol. 332, pp. 25–30, 2015.

[90] Y. G. Hur, D. W. Lee, and K. Y. Lee, “Hydrocracking of vacuum residue using NiWS(x) dispersed catalysts,” *Fuel*, vol. 185, pp. 794–803, 2016.

[91] R. Tiwari *et al.*, “Hydrotreating and hydrocracking catalysts for processing of waste soya-oil and refinery-oil mixtures,” *Catal. Commun.*, vol. 12, no. 6, pp. 559–562, 2011.

[92] R. Silva-Rodrigo, C. Calderón-Salas, J. A. Melo-Banda, J. M. Domínguez, and A. Vázquez-Rodríguez, “Synthesis, characterization and comparison of catalytic properties of NiMo- and NiW/Ti-MCM-41 catalysts for HDS of thiophene and HVGO,” *Catal. Today*, vol. 98, no. 1-2 SPEC. ISS., pp. 123–129, 2004.

[93] C. Leyva, M. S. Rana, F. Trejo, and J. Ancheyta, “NiMo supported acidic catalysts for heavy oil hydroprocessing,” *Catal. Today*, vol. 141, no. 1–2, pp. 168–175, 2009.

[94] A. Carlsson, M. Brorson, and H. Topsøe, “Morphology of WS2nanoclusters in WS2/C hydrodesulfurization catalysts revealed by high-angle annular dark-field scanning transmission electron microscopy (HAADF-STEM) imaging,” *J. Catal.*, vol. 227, no. 2, pp. 530–536, 2004.

[95] J. Li *et al.*, “Hydrodemetallation (HDM) of nickel-5,10,15,20-tetraphenylporphyrin (Ni-TPP) over NiMo/γ-Al 2O 3 catalyst prepared by one-pot method with controlled precipitation of the components,” *Fuel*, vol. 97, pp. 504–511, 2012.

[96] E. Furimsky and F. E. Massoth, “Deactivation of Hydroprocessing Catalysts,” *Catal. Today*, vol. 52, pp. 381–495, 1999.

[97] H. J. Eom, D. W. Lee, S. Kim, S. H. Chung, Y. G. Hur, and K. Y. Lee, “Hydrocracking of extra-heavy oil using Cs-exchanged phosphotungstic acid (CsxH3-xPW12O40, x = 1-3) catalysts,” *Fuel*, vol. 126, pp. 263–270, 2014.

[98] N. Panariti, A. Del Bianco, G. Del Piero, and M. Marchionna, “Petroleum residue upgrading with dispersed catalysts Part 1. Catalysts activity and selectivity,” *Appl. Catal. A Gen.*, vol. 204, pp. 203–213, 2000.

[99] I. Watanabe, M. Otake, M. Yoshimoto, K. Sakanishi, Y. Korai, and I. Mochida, “Behaviors of oil-soluble molybdenum complexes to form very fine MoS2 particles in vacuum residue,” *Fuel*, vol. 81, pp. 1515–1520, 2002.

[100] C. Ovalles, E. Filgueiras, A. Morales, C. E. Scott, F. Gonzalez-Gimenez, and B. Pierre Embaid, “Use of a dispersed iron catalyst for upgrading extra-heavy crude oil using methane as source of hydrogen,” *Fuel*, vol. 82, no. 8, pp. 887–892, 2003.

[101] S. G. Jeon, J. G. Na, C. H. Ko, K. B. Lee, N. S. Rho, and S. Bin Park, “A new approach for preparation of oil-soluble bimetallic dispersed catalyst from layered ammonium nickel molybdate,” *Mater. Sci. Eng. B Solid-State Mater. Adv. Technol.*, vol. 176, no. 7, pp. 606–610, 2011.

[102] D. Genuit, P. Afanasiev, and M. Vrinat, “Solution syntheses of unsupported Co(Ni)-Mo-S hydrotreating catalysts,” *J. Catal.*, vol. 235, no. 2, pp. 302–317, 2005.

[103] W. Liu, Y. Du, B. Qin, F. Wang, X. Zhang, and H. Gao, “Hydrocracking Catalyst, Preperation Method and Use Thereof, and Method for Hydrocracking Catalytic Diesel Oil,” EP 3 168 283 A1, 2017.

[104] G. Yu, S. Lu, H. Chen, and Z. Zhu, “Diesel fuel desulfurization with hydrogen peroxide promoted by formic acid and catalyzed by activated carbon,” vol. 43, pp. 2285–2294, 2005.

[105] C. P. Veeramalai, F. Li, H. Xu, T. W. Kim, and T. Guo, “One pot hydrothermal synthesis of graphene like MoS2 nanosheets for application in high performance lithium ion batteries,” *R. Soc. Chem.*, vol. 5, no. July, pp. 57666–57670, 2015.

[106] H. Xia, M. Lai, and L. Lu, “Nanoflaky MnO2/carbon nanotube nanocomposites as anode materials for lithium-ion batteries,” *J. Mater. Chem.*, vol. 20, pp. 6896–6902, 2010.

[107] B. Luo and L. Zhi, “Design and construction of three dimensional graphene-based composites for lithium ion battery applications,” *Energy Environ. Sci.*, vol. 00, no. December, pp. 1–22, 2014.

[108] H. Liu, J. Huang, X. Li, J. Liu, Y. Zhang, and K. Du, “Flower-like SnO 2 / graphene composite for high-capacity lithium storage,” *Appl. Surf. Sci.*, vol. 258, no. 11, pp. 4917–4921, 2012.

[109] C. Ge *et al.*, “Three-dimensional flower-like nickel oxide supported on graphene sheets as electrode material for supercapacitors,” *J. Sol-Gel Sci. Technol.*, vol. 63, pp. 146–152, 2012.

[110] L. Zhang, G. Du, B. Zhou, and L. Wang, “Green synthesis of fl ower-like ZnO decorated reduced graphene oxide composites,” *Ceram. Int.*, vol. 40, no. 1, pp. 1241–1244, 2014.

[111] J. S. J. Hargreaves and A. L. Munnoch, “A survey of the influence of binders in zeolite catalysis,” *Catal. Sci. Technol.*, vol. 3, no. 5, pp. 1165–1171, 2013.

[112] P. S. F. Mendes, J. M. Silva, M. F. Ribeiro, A. Daudin, and C. Bouchy, “From powder to extrudate zeolite-based bifunctional hydroisomerization catalysts: on preserving zeolite integrity and optimizing Pt location,” *J. Ind. Eng. Chem.*, vol. 62, pp. 72–83, 2018.

[113] M. Li, Y. Zhang, H. Wang, S. Yu, D. Liu, and Y. Wang, “Influence of zeolite crystal size on selective conversion of n-alkane: Controlling intermediates’ diffusion distances inside the micropores,” *Fuel*, vol. 254, no. May, 2019.

[114] A. De Lucas, M. J. Ramos, F. Dorado, P. Sánchez, and J. L. Valverde, “Influence of the Si/Al ratio in the hydroisomerization of n-octane over platinum and palladium beta zeolite-based catalysts with or without binder,” *Appl. Catal. A Gen.*, vol. 289, no. 2, pp. 205–213, 2005.

[115] P. Sánchez, F. Dorado, M. J. Ramos, R. Romero, V. Jiménez, and J. L. Valverde, “Hydroisomerization of C6-C8 n-alkanes, cyclohexane and benzene over palladium and platinum beta catalysts agglomerated with bentonite,” *Appl. Catal. A Gen.*, vol. 314, no. 2, pp. 248–255, 2006.

[116] Z. Vajglová *et al.*, “Effect of the Preparation of Pt-Modified Zeolite Beta-Bentonite Extrudates on Their Catalytic Behavior in n-Hexane Hydroisomerization,” *Ind. Eng. Chem. Res.*, 2019.

[117] J. Harmel, L. I. Van Der Wal, J. Zečević, P. E. De Jongh, and K. P. De Jong, “Influence of intimacy for metal-mesoporous solid acids catalysts for: N -alkanes hydro-conversion,” *Catal. Sci. Technol.*, vol. 10, no. 7, pp. 2111–2119, 2020.

[118] X. Kong and J. Liu, “Influence of alumina binder content on catalytic performance of Ni/HZSM-5 for hydrodeoxygenation of cyclohexanone,” *PLoS One*, vol. 9, no. 7, pp. 5–10, 2014.

[119] X. Du, X. Kong, and L. Chen, “Influence of binder on catalytic performance of Ni/HZSM-5 for hydrodeoxygenation of cyclohexanone,” *Catal. Commun.*, vol. 45, no. June, pp. 109–113, 2014.

[120] S. Raseev, *Hydrocracking in Thermal and Catalytic Processes in Petroleum refining*. Marcel Dekker Inc., 2003.

[121] J. W. Thybaut and G. B. Marin, “Testing of Catalytic Properties,” in *Catalysis, Encyclopedia of Life Support Systems*, G. Centi, Ed. Oxford: Eolss Publishers, 2009.

[122] C. Pirola, I. Rossetti, and V. Ragaini, “Are Conversion , Selectivity and Yield terms unambiguously defined in Chemical and Chemical Engineering terminology?,” *Sci. Technol.*, 2006.

[123] S. Parkash, “Hydrocracking Processes,” in *Refining Processes Handbook*, Elsevier, 2003, pp. 62–108.

[124] Y. S. Kim, K. S. Cho, and Y. K. Lee, “Morphology effect of B-zeolite supports for Ni2P catalysts on the hydrocracking of polycyclic aromatic hydrocarbons to benzene, toluene, and xylene,” *J. Catal.*, vol. 351, pp. 67–78, 2017.

[125] Y. S. Kim, G. N. Yun, and Y. K. Lee, “Novel Ni2P/zeolite catalysts for naphthalene hydrocracking to BTX,” *Catal. Commun.*, vol. 45, pp. 133–138, 2014.

[126] N. H. R. Annuar, S. Triwahyono, A. A. Jalil, N. Basar, T. A. T. Abdullah, and A. Ahmad, “Effect of Cr2O3 loading on the properties and cracking activity of Pt/Cr2O3-ZrO2,” *Appl. Catal. A Gen.*, vol. 541, no. March, pp. 77–86, 2017.

[127] L. Zhu, F. S. Xiao, Z. Zhang, Y. Sun, Y. Han, and S. Qiu, “High activity in catalytic cracking over stable mesoporous aluminosilicates,” *Catal. Today*, vol. 68, no. 1–3, pp. 209–216, 2001.

[128] Y. Oh *et al.*, “Selective hydrotreating and hydrocracking of FCC light cycle oil into high-value light aromatic hydrocarbons,” *Appl. Catal. A Gen.*, vol. 577, no. February, pp. 86–98, 2019.

[129] G. C. Laredo, P. Pérez-Romo, J. Escobar, J. L. Garcia-Gutierrez, and P. M. Vega-Merino, “Light cycle oil upgrading to benzene, toluene, and xylenes by hydrocracking: Studies

using model mixtures," *Ind. Eng. Chem. Res.*, vol. 56, no. 39, pp. 10939–10948, 2017.

[130] G. V. Butley *et al.*, "Integrated process for production of high octane gasoline, high aromatic naphtha and high cetane diesel from high aromatic middle distillate range streams," US9644155B2, 2015.

[131] A. J. M. Oprins, "Integrated hydrocracking process," US9850438B2, 2017.

[132] Y. Zhang, T. L. M. Maesen, Y. Hao, D. R. Bushee, and T. M. Rea, "Middle distillate hydrocracking catalyst containing zeolite beta with low od acidity and large domain size," US20170043328A1, 2016.

[133] Y. Zhang, T. L. M. Maesen, Y. Hao, and T. M. Rea, "Middle distillate hydrocracking catalyst containing zeolite USY, and zeolite beta with low acidity and large domain size," US10040058B2, 2017.

[134] J. Jia, A. Rainis, T. L. M. Maesen, R. Coser, and Y. Zhang, "Noble metal zeolite catalyst for second-stage hydrocracking," US20160214094A1, 2016.

[135] J. Shin, Y. Oh, Y. Choi, J. Lee, and J. K. Lee, "Design of selective hydrocracking catalysts for BTX production from diesel-boiling-range polycyclic aromatic hydrocarbons," *Appl. Catal. A Gen.*, vol. 547, no. August, pp. 12–21, 2017.

[136] J. Lee, Y. Choi, J. Shin, and J. K. Lee, "Selective hydrocracking of tetralin for light aromatic hydrocarbons," *Catal. Today*, vol. 265, pp. 144–153, 2016.

[137] S. G. A. Ferraz, F. M. Z. Zotin, L. R. R. Araujo, and J. L. Zotin, "Influence of support acidity of NiMoS catalysts in the activity for hydrogenation and hydrocracking of tetralin," *Appl. Catal. A Gen.*, vol. 384, no. 1–2, pp. 51–57, 2010.

[138] L. Wang *et al.*, "Upgrading of light cycle oil via coupled hydrogenation and ring-opening over NiW/Al2O3-USY catalysts," *Catal. Today*, vol. 158, no. 3–4, pp. 343–347, 2010.

[139] Y. Wang, B. Shen, L. Wang, B. Feng, J. Li, and Q. Guo, "Effect of phosphorus modified USY on coupled hydrogenation and ring opening performance of NiW/USY+Al2O3 hydro-upgrading catalyst," *Fuel Process. Technol.*, vol. 106, pp. 141–148, 2013.

[140] D. Santi, T. Holl, V. Calemma, and J. Weitkamp, "High-performance ring-opening catalysts based on iridium-containing zeolite Beta in the hydroconversion of decalin," *Appl. Catal. A Gen.*, vol. 455, pp. 46–57, 2013.

[141] J. Quinchia, J. Sánchez, J. C. Poveda, and A. Moreno, "Microwave-assisted synthesis of mesostructured aluminosilicates (MA) for the preparation of nano-MoS2/MA catalysts active in decalin hydrocracking," *Microporous Mesoporous Mater.*, vol. 301, p. 110226, 2020.

[142] C. Peng *et al.*, "Direct production of high octane gasoline and ULSD blend stocks by LCO hydrocracking," *Catal. Today*, vol. 271, pp. 149–153, 2016.

[143] C. Peng, X. chen Fang, R. hui Zeng, R. Guo, and W. yue Hao, "Commercial analysis of

catalytic hydroprocessing technologies in producing diesel and gasoline by light cycle oil," *Catal. Today*, vol. 276, pp. 11–18, 2016.

[144] Z. Cao *et al.*, "Selective hydrocracking of light cycle oil into high-octane gasoline over bi-functional catalysts," *J. Energy Chem.*, vol. 52, pp. 41–50, 2020.

[145] C. Peng, B. Liu, X. Feng, Y. Du, and X. Fang, "Engineering dual bed hydrocracking catalyst towards enhanced high-octane gasoline generation from light cycle oil," *Chem. Eng. J.*, vol. 389, p. 123461, 2020.

[146] V. Calemma, M. Ferrari, S. Rabl, and J. Weitkamp, "Selective ring opening of naphthenes: From mechanistic studies with a model feed to the upgrading of a hydrotreated light cycle oil," *Fuel*, vol. 111, pp. 763–770, 2013.

[147] S. Akmaz and P. A. Caglayan, "Effect of catalyst, temperature, and hydrogen pressure on slurry hydrocracking reactions of naphthalene," *Chem. Eng. Technol.*, vol. 38, no. 5, pp. 917–930, 2015.

[148] D. P. Upare *et al.*, "Selective hydrocracking of pyrolysis fuel oil into benzene, toluene and xylene over CoMo/beta zeolite catalyst," *J. Ind. Eng. Chem.*, vol. 46, pp. 356–363, 2017.

[149] C. Manrique, A. Guzmán, J. Pérez-Pariente, C. Márquez-Álvarez, and A. Echavarría, "Vacuum gas-oil hydrocracking performance of Beta zeolite obtained by hydrothermal synthesis using carbon nanotubes as mesoporous template," *Fuel*, vol. 182, no. 53, pp. 236–247, 2016.

[150] Q. Zhao *et al.*, "Core-shell structured zeolite-zeolite composites comprising Y zeolite cores and nano-β zeolite shells: Synthesis and application in hydrocracking of VGO oil," *Chem. Eng. J.*, vol. 257, pp. 262–272, 2014.

[151] E. Van Kimmenade and L. Aramburo, "Process for combined hydrodesulfurization and hydrocracking of heavy hydrocarbons," WO 2017/144438 Al, 2017.

[152] C. Liu, F. Wang, M. Guan, Y. Du, W. Huang, and H. Zhao, "Na-Y Molecular Sieve, H-Y Molecular Sieve, and Preparation Methods Thereof, Hydrocracking Catalyst, and Hydrocracking Method," US 2016/0151771 A1, 2016.

[153] A. B. Dandekar, J. R. McManus, and K. Wilson, "Jet and Diesel Selective Hydrocracking," US 2017 / 0335207 A1, 2017.

[154] S. Kannaiyan, V. R. Madhavan, S. Rajagopal, and A. Jayabalan, "An experimental analysis on tar cracking using nano structured Ni-Co/Si-P catalyst in a biomass gasifier-based power generating system," *Appl. Therm. Eng.*, vol. 97, pp. 13–21, 2016.

[155] J. E. Patiño and F. B. Cortés, "Nanocatalysts for hydrocracking and methods of their use," US9339796B2, 2016.

[156] K. H. Kang, G. T. Kim, S. Park, P. W. Seo, H. Seo, and C. W. Lee, "A review on the Mo-precursors for catalytic hydroconversion of heavy oil," *J. Ind. Eng. Chem.*, vol. 76, pp. 1–16, 2019.

[157] J. L. Agudelo, E. J. M. Hensen, S. A. Giraldo, and L. J. Hoyos, “Influence of steam-calcination and acid leaching treatment on the VGO hydrocracking performance of faujasite zeolite,” *Fuel Process. Technol.*, vol. 133, pp. 89–96, 2015.

[158] U. Ghosh, K. Kulkarni, A.D.Kulkarni, and P.L.Chaudhari, “Review – Hydrocracking using Different Catalysts,” *Chem. Process Eng. Res.*, vol. 34, no. June, pp. 51–56, 2015.

[159] M. O. Kazakov *et al.*, “Hydrocracking of vacuum gas oil over NiMo/Y-Al2O3: Effect of mesoporosity introduced by zeolite Y recrystallization,” *Catal. Today*, vol. 305, no. August 2017, pp. 117–125, 2018.

[160] P. P. Dik *et al.*, “Hydrocracking of vacuum gas oil over NiMo/zeolite-Al2O3: Influence of zeolite properties,” *Fuel*, vol. 237, no. September 2018, pp. 178–190, 2019.

[161] Q. Cui *et al.*, “Synthesis and characterization of Zr incorporated small crystal size Y zeolite supported NiW catalysts for hydrocracking of vacuum gas oil,” *Fuel*, vol. 237, no. April 2018, pp. 597–605, 2019.

[162] C. M. Halmenschlager, M. Brar, I. T. Apan, and A. de Klerk, “Hydrocracking vacuum gas oil with wax,” *Catal. Today*, no. June, pp. 1–10, 2019.

[163] S. Shin *et al.*, “Synthesis of noble molybdenum and tungsten complexes for hydrocracking catalyst of heavy oil,” *J. Ind. Eng. Chem.*, vol. 72, pp. 408–413, 2019.

[164] K. H. Kang *et al.*, “Slurry-phase hydrocracking of heavy oil over Mo precursors: Effect of triphenylphosphine ligands,” *J. Catal.*, vol. 384, pp. 106–121, 2020.

[165] L. I. Chuan, S. H. I. Bin, C. U. I. Min, S. Hong-yan, and Q. U. E. Guo-he, “Application of Co-Mo / CNT catalyst in hydro-cracking of Gudao vacuum residue,” vol. 35, no. 4, 2007.

[166] Y. Yue *et al.*, “From cheap natural bauxite to high-efficient slurry-phase hydrocracking catalyst for high temperature coal tar: A simple hydrothermal modification,” *Fuel Process. Technol.*, vol. 175, no. March, pp. 123–130, 2018.

[167] M. Majka, G. Tomaszewicz, and A. Mianowski, “Experimental study on the coal tar hydrocracking process over different catalysts,” *J. Energy Inst.*, vol. 91, no. 6, pp. 1164–1176, 2018.

[168] R. Saab, K. Polychronopoulou, N. Charisiou, M. A. Goula, and A. Schiffer, “Graphene Nanoplatelets-Based Ni-Zeolite Composite Catalysts for Heptane Hydrocracking,” *C*, vol. 6, no. 31, 2020.

[169] S. Fatima, G. Singaravel, and R. Hashaikeh, “Ni-W/nano zeolite Y catalysts for n-heptane hydrocracking,” *Mater. Chem. Phys.*, vol. 212, pp. 87–94, 2018.

[170] S. F. Anis, G. Singaravel, and R. Hashaikeh, “Hierarchical nano zeolite-Y hydrocracking composite fibers with highly efficient hydrocracking capability,” *RSC Adv.*, vol. 8, no. 30, pp. 16703–16715, 2018.

[171] Saepurahman and R. Hashaikeh, “Insight into ball milling for size reduction and

nanoparticles production of H-Y zeolite," *Mater. Chem. Phys.*, vol. 220, pp. 322–330, 2018.

[172] O. K. Krasilnikova, E. B. Markova, T. Y. Grankina, E. V. Khozina, and V. N. Simonov, "Influence of Self-organization of Al2O3 and TiO2/Al2O3 Nanofilaments into Nanotubes Caused by High Temperature Hydrogen Treatment on Propane Cracking," *Nanosci. &Nanotechnology-Asia*, vol. 8, no. 1, pp. 100–115, 2018.

[173] J. A. Martens, D. Verboekend, K. Thomas, G. Vanbutsele, J. Pérez-Ramírez, and J. P. Gilson, "Hydroisomerization and hydrocracking of linear and multibranched long model alkanes on hierarchical Pt/ZSM-22 zeolite," *Catal. Today*, vol. 218–219, pp. 135–142, 2013.

[174] E. Verheyen *et al.*, "Molecular shape-selectivity of MFI zeolite nanosheets in n-decane isomerization and hydrocracking," *J. Catal.*, vol. 300, pp. 70–80, 2013.

[175] I. Rossetti, C. Gambaro, and V. Calemma, "Hydrocracking of long chain linear paraffins," *Chem. Eng. J.*, vol. 154, no. 1–3, pp. 295–301, 2009.

[176] M. Hasan, A. M. Mohamed, and H. Al-Kandari, "Semi-industrial studies of Tungsten-based catalyst for hydroisomerization/hydrocracking of n-hexane and n-heptane," *Mol. Catal.*, vol. 452, no. January, pp. 1–10, 2018.

[177] M. O. Kazakov *et al.*, "Influence of USY Zeolite Recrystallization on Physicochemical Properties and Catalytic Performance of NiMo/USY-Al2O3 Hydrocracking Catalysts," *Catal. Today*, 2019.

[178] T. Kaka khel *et al.*, "Hexadecane hydrocracking for production of jet fuels from renewable diesel over proton and metal modified H-Beta zeolites," *Mol. Catal.*, vol. 476, no. March, p. 110515, 2019.

[179] T. Imyen, W. Wannapakdee, J. Limtrakul, and C. Wattanakit, "Role of hierarchical micro-mesoporous structure of ZSM-5 derived from an embedded nanocarbon cluster synthesis approach in isomerization of alkenes, catalytic cracking and hydrocracking of alkanes," *Fuel*, vol. 254, no. May, p. 115593, 2019.

[180] J. Francis, E. Guillon, N. Bats, C. Pichon, A. Corma, and L. J. Simon, "Design of improved hydrocracking catalysts by increasing the proximity between acid and metallic sites," *Appl. Catal. A Gen.*, vol. 409–410, pp. 140–147, 2011.

[181] H. Amirmoghadam, M. H. Sadr, H. Aghabozorg, F. Salehirad, and A. Irandoukht, "The effect of molybdenum on the characteristics and catalytic properties of M/Cs1.5H1.5PW12O40/Al2O3 (M = Ni or/and Mo) nanocatalysts in the hydrocracking of n-decane," *React. Kinet. Mech. Catal.*, vol. 125, no. 2, pp. 983–994, 2018.

[182] T. Li, J. Cheng, R. Huang, W. Yang, J. Zhou, and K. Cen, "Hydrocracking of palm oil to jet biofuel over different zeolites," *Int. J. Hydrogen Energy*, vol. 41, no. 47, pp. 21883–21887, 2016.

[183] S. Liu, Q. Zhu, Q. Guan, L. He, and W. Li, "Bio-aviation fuel production from

hydroprocessing castor oil promoted by the nickel-based bifunctional catalysts," *Bioresour. Technol.*, vol. 183, pp. 93–100, 2015.

[184] J. Liu, K. Fan, W. Tian, C. Liu, and L. Rong, "Hydroprocessing of Jatropha oil over NiMoCe/Al2O3catalyst," *Int. J. Hydrogen Energy*, vol. 37, no. 23, pp. 17731–17737, 2012.

[185] A. E. Barrón C. *et al.*, "Catalytic hydrocracking of vegetable oil for agrofuels production using Ni-Mo, Ni-W, Pt and TFA catalysts supported on SBA-15," *Catal. Today*, vol. 166, no. 1, pp. 102–110, 2011.

[186] A. Ishihara, N. Fukui, H. Nasu, and T. Hashimoto, "Hydrocracking of soybean oil using zeolite-alumina composite supported NiMo catalysts," *Fuel*, vol. 134, pp. 611–617, 2014.

[187] B. Veriansyah *et al.*, "Production of renewable diesel by hydroprocessing of soybean oil: Effect of catalysts," *Fuel*, vol. 94, pp. 578–585, 2012.

[188] H. Jeong, M. Shin, B. Jeong, J. H. Jang, G. B. Han, and Y. W. Suh, "Comparison of activity and stability of supported Ni2P and Pt catalysts in the hydroprocessing of palm oil into normal paraffins," *J. Ind. Eng. Chem.*, vol. 83, pp. 189–199, 2020.

[189] P. Šimáček, D. Kubička, G. Šebor, and M. Pospíšil, "Hydroprocessed rapeseed oil as a source of hydrocarbon-based biodiesel," *Fuel*, vol. 88, no. 3, pp. 456–460, 2009.

[190] T. M. Sankaranarayanan, M. Banu, A. Pandurangan, and S. Sivasanker, "Hydroprocessing of sunflower oil-gas oil blends over sulfided Ni-Mo-Al-zeolite beta composites," *Bioresour. Technol.*, vol. 102, no. 22, pp. 10717–10723, 2011.

[191] M. Krár, S. Kovács, D. Kalló, and J. Hancsók, "Fuel purpose hydrotreating of sunflower oil on CoMo/Al2O3catalyst," *Bioresour. Technol.*, vol. 101, no. 23, pp. 9287–9293, 2010.

[192] A. Ishihara, R. Ishida, T. Ogiyama, H. Nasu, and T. Hashimoto, "Dehydrocyclization-cracking reaction of soybean oil using zeolite-metal oxide composite-supported PtNiMo sulfided catalysts," *Fuel Process. Technol.*, vol. 161, pp. 17–22, 2017.

[193] Z. Zhang, J. Cheng, Y. Zhu, H. Guo, and W. Yang, "Jet fuel range hydrocarbons production through competitive pathways of hydrocracking and isomerization over HPW-Ni/MCM-41 catalyst," *Fuel*, vol. 269, no. February, p. 117465, 2020.